NASA TN D-217

TECHNICAL NOTE
D-217

LOW-SPEED INVESTIGATION OF STATIC LONGITUDINAL AND LATERAL STABILITY CHARACTERISTICS OF AN AIRPLANE CONFIGURATION WITH A HIGHLY TAPERED WING AND WITH SEVERAL BODY AND TAIL ARRANGEMENTS

By Paul G. Fournier

Langley Research Center
Langley Field, Va.

NATIONAL AERONAUTICS AND SPACE ADMINISTRATION

WASHINGTON

January 1960

NATIONAL AERONAUTICS AND SPACE ADMINISTRATION

TECHNICAL NOTE D-217

LOW-SPEED INVESTIGATION OF STATIC LONGITUDINAL AND LATERAL STABILITY CHARACTERISTICS OF AN AIRPLANE CONFIGURATION WITH A HIGHLY TAPERED WING AND WITH SEVERAL BODY AND TAIL ARRANGEMENTS[1]

By Paul G. Fournier

SUMMARY

A low-speed investigation was made in the Langley 300 MPH 7- by 10-foot tunnel of the static longitudinal and lateral stability characteristics of an airplane model with multiple bodies and of a conventional (single-fuselage) model in combination with a wing of aspect ratio 4. The wing had zero sweep at the 80-percent-chord line, a taper ratio of zero, and an NACA 65A004 airfoil section. Several tail arrangements were tested with the three-body configuration along with a conventional-tail arrangement for both models. The results indicate that the pitching-moment characteristics for the three-body model appear to bear about the same relation to height of the horizontal tail as that which has been well established by previous investigations of conventional (single-fuselage) configurations. It appears that acceptable longitudinal stability can be obtained for both complete model configurations with the horizontal tail located in or near the wing-chord plane.

The data show that for the multiple-body (three-body) model all tail-on configurations were directionally stable throughout the angle-of-attack range and were greatly improved over the conventional model configuration which was directionally unstable above an angle of attack of 20°. The data also indicate that this improved directional stability for the complete three-body model results from the fact that with the tail off the directional stability becomes positive at high angles of attack.

---

[1]Supersedes recently declassified NACA Research Memorandum L57A08 by Paul G. Fournier, 1957.

INTRODUCTION

The conventional arrangement of current high-speed airplane configurations, in which the total required volume is contained primarily within a single long slender body to which the stabilizing surfaces are also attached, imposes certain objectionable flight characteristics as well as some undesirable operational limitations. With such configurations directional stability has been difficult to maintain at high angles of attack (ref. 1), whereas a considerable amount of directional stability is required to avoid serious divergence problems due to roll coupling in an airplane with a concentration of mass along the body (ref. 2). Incompatibility of engine and armament operation, stores release, and speed-brake installation are also complications encountered with a single slender fuselage.

The three-body arrangement investigated herein was conceived as a possible means for alleviating the problems mentioned in the preceding paragraph while maintaining an arrangement that would appear to entail no serious compromise in high-speed performance capabilities. Consideration of essentially the same general philosophy, but with emphasis on the improvement of high-lift longitudinal stability, provided the basis for the investigation reported in reference 3. For the test model, the total body volume was divided equally among three separate bodies - one which extends forward of the wing in the plane of symmetry and two which extend rearward from the wing at outboard locations. The wing had an aspect ratio of 4, a taper ratio of zero, and zero sweep at the 0.80-chord line. The tests covered several configurations of tails attached to the outboard bodies. Static longitudinal and lateral stability characteristics for the various arrangements of the model were determined at low speeds. For comparison purposes, the wing of the investigation was also tested in a conventional fuselage and tail arrangement.

COEFFICIENTS AND SYMBOLS

The axis system used and the direction of positive forces, moments, and angles are presented in figure 1. All moments of the basic data are referred to the quarter-chord point of the wing mean aerodynamic chord, and except for lift and drag all data are presented about the body axis.

b wing span, ft

C_D drag coefficient, $\frac{\text{Drag}}{qS}$

C_L lift coefficient, $\frac{\text{Lift}}{qS}$

C_l rolling-moment coefficient, $\frac{\text{Rolling moment}}{qSb}$

C_m pitching-moment coefficient, $\frac{\text{Pitching moment}}{qS\bar{c}}$

C_n yawing-moment coefficient, $\frac{\text{Yawing moment}}{qSb}$

C_Y lateral-force coefficient, $\frac{\text{Lateral force}}{qS}$

C_{l_β} rolling moment due to sideslip, $\frac{\partial C_l}{\partial \beta}$, per deg

C_{n_β} yawing moment due to sideslip, $\frac{\partial C_n}{\partial \beta}$, per deg

C_{Y_β} lateral force due to sideslip, $\frac{\partial C_Y}{\partial \beta}$, per deg

c wing chord, ft

$\bar{c}$ wing mean aerodynamic chord, ft

l fuselage or body length, in.

q free-stream dynamic pressure, $\frac{\rho V^2}{2}$, lb/sq ft

S wing area, sq ft

V free-stream velocity, ft/sec

α angle of attack, deg

β angle of sideslip, deg

ρ mass density of air, slugs/cu ft

$\Lambda_{c/4}$ sweep of the quarter-chord line, deg

ΔC_{n_β} increment of C_{n_β} due to vertical tail (complete model data minus wing-fuselage data)

TESTS AND CORRECTIONS

All tests were made at a dynamic pressure of 45.85 pounds per square foot, which for average test condition corresponds to a Mach number of about 0.18 and a Reynolds number of 1.85×10^6 based on the wing mean aerodynamic chord of 1.479 feet.

The present investigation consists of tests made to determine the low-speed static longitudinal and lateral stability characteristics of a three-body model as compared with a conventional (single-fuselage) model. The angle-of-attack range was from approximately -4° to between 26° and 36°, depending on the configuration. The parameters C_{l_β}, C_{n_β}, and C_{Y_β} were determined from tests at sideslip angles of $\pm 5^\circ$ throughout the angle-of-attack range. The angle of attack, drag, and pitching moment with the horizontal tail on have been corrected for jet-boundary effects as well as for blockage effects on the dynamic pressure and drag coefficient in accordance with standard procedures.

Vertical buoyancy on the support strut, tunnel-airflow misalinement, and longitudinal pressure gradient have been accounted for in the computation of the data. These data have not been corrected for the tares caused by the model-support strut; however, tare tests of a complete model similar to the conventional model of the present investigation have indicated that tares corresponding to the lateral coefficients are small, that the correction to drag coefficient is about 0.009 at zero lift, and that the correction to pitching-moment coefficient is small and independent of angle of attack through most of the range. It is felt that the tare corrections for the three-body model would be still smaller, inasmuch as there is no fuselage directly rearward of the model-support strut.

MODEL AND APPARATUS

The wing of the present investigation had an aspect ratio of 4, a taper ratio of zero, an NACA 65A004 airfoil section parallel to the plane of symmetry, and zero sweep at the 80-percent-chord line $\left(\Lambda_{c/4} = 28.80^\circ\right)$. The wing was fabricated from 0.5-inch aluminum-alloy plate bonded with wood and machined to give the desired airfoil.

The three bodies as well as the single fuselage were constructed of mahogany. The three-body model was constructed so that the total volume of the three bodies is the same as that of the single fuselage. For ease of construction all three bodies were made identical, the small fairing at the rear of the center body was added later. The ordinates

of the single fuselage and of one body of the three-body model are presented in tables I and II, respectively. Three-view drawings of the three-body model and the conventional model are presented in figure 2. A photograph of the complete three-body model with a T-tail arrangement is shown in figure 3.

The horizontal- and vertical-tail surfaces used with the three-body model were made of 0.250-inch aluminum alloy, with rounded leading edges and tapered trailing edges. The horizontal-tail surface for the conventional model was of the same plan form as the wing but was made of 0.375-inch aluminum alloy with rounded leading edge and tapered trailing edge, whereas the vertical tail had an aspect ratio of 1.16 with an NACA 63A009 airfoil section. Sketches of all the tail arrangements used are presented in figure 4. Details of additional tail assemblies other than the one shown in figure 2(a) for the three-body model are presented in figures 2(c) and (d). All horizontal tails had zero incidence.

The three-body model was so constructed that the wing could be tested alone or with any symmetrical combination of the three bodies. The wing of this investigation was in a midwing position and was mounted so that moments and forces were measured about the quarter-chord of the wing mean aerodynamic chord.

The model was mounted on a single support strut which in turn was attached to the mechanical-balance system of the Langley 300 MPH 7- by 10-foot tunnel.

RESULTS AND DISCUSSION

Presentation of Results

The results of the present investigation are presented in figures 5 to 32. The longitudinal characteristics of the three-body model with various tail arrangements are found in figures 5 to 14. A summary of the effect of the tail and body arrangements on the longitudinal characteristics is presented in figure 15. The variations of lateral data are shown in figures 16 to 32.

Longitudinal Stability Characteristics

The basic static longitudinal stability results presented in figures 5 to 14 represent a center-of-gravity location at the $0.25\bar{c}$ location. The static margin therefore varied somewhat with the different configurations. In order to provide a more realistic comparison of the pitching-moment curves, the data in the summary plots (fig. 15) have

been recomputed with respect to a center-of-gravity location such that a static margin of $0.10\bar{c}$ is obtained for all configurations at zero lift.

In general, figures 15(a) and (b) show that the pitching-moment characteristics of the three-body model are less favorable for the high-tail positions than for the case of the tail in the wing-chord plane. These results show very much the same trends with tail height as those established for conventional (single-fuselage) configurations (ref. 4) and result primarily from the downwash characteristics behind the wing. Of the tails above the wing-chord plane, only the inverted V-tail (tail 6) showed no reduction in stability at high lift. The configuration with tail 6 provided the most nearly linear pitching-moment curves obtained in the investigation (fig. 15); however, as is indicated in a subsequent section, the directional characteristics were rather poor for this configuration.

Figures 15(c) and (d) show comparisons of the longitudinal stability of the three-body model with various tail arrangements and with the conventional single-fuselage model for the complete and tail-off configurations. The results indicate that there are several possible tail arrangements with the three-body model that provide pitching-moment characteristics comparable to those of the single-fuselage model with a low tail. The three-body configurations with the cruciform tail (tail 1) or the modified cruciform tail with the inboard portion of the horizontal tail removed (tail 4) experienced rather rapid increases in stability at $\alpha = 7^\circ$ and some reduction in stability above $\alpha \approx 26^\circ$ (fig. 15(c)); however, these nonlinearities do not appear serious. The wing-fuselage configurations shown in figure 15(d) indicate that both the three-body model and the conventional single-fuselage model exhibited reasonably linear pitching-moment characteristics throughout the angle-of-attack range, and that the three-body model provided a somewhat higher value of maximum lift coefficient. In general, it may be noted that for the tail incidence tested (0°), the three-body configuration (figs. 15(c) and (d)) provided higher values of trim lift coefficient than the conventional configuration.

Lateral Stability Characteristics

The effects on the static lateral stability derivatives of the addition of different arrangements of bodies to the wing with an aspect ratio of 4 are shown in figure 30. Although the wing alone has almost neutral directional stability, the addition of the conventional fuselage made the configuration directionally unstable throughout the angle-of-attack range with a region of very high instability between an angle of attack of 17° and of 25°. The wing plus the center body of the three-body model were also directionally unstable; however, the large

dip found in the C_{n_β} curve for the conventional wing-fuselage configuration was absent. The presence of the region of high instability for the conventional configuration and its absence for the configuration with the single center body is an indication of the adverse effect of the wing-induced sidewash on a fuselage afterbody as has been pointed out in reference 5. It is of interest to note that when the two outer bodies were added to the wing plus the center body the directional instability at low angles of attack was about the same as for the conventional model; however, as the angle of attack increased, the instability diminished for the three-body model. Above $\alpha = 15^\circ$ the three-body model was stable with tail off.

A positive dihedral effect $\left(-C_{l_\beta}\right)$ was noted for the wing alone and for the three-body configurations throughout the angle-of-attack range (fig. 30). Both the conventional and the single-center-body configuration indicated a negative dihedral effect above $\alpha = 16^\circ$, the latter showing a large value at $\alpha = 25^\circ$.

The static lateral stability data (figs. 17 to 29) indicate that the directional stability characteristics of all the complete configurations of the three-body model were improved over those of the conventional complete-model configuration; that is, all the three-body configurations were directionally stable throughout the angle-of-attack range, although for some the stability was marginal (tails 6 and 9). Two of the best configurations, one with the cruciform tail (tail 1) and one with the conventional vertical tail (tail 3), are compared with the conventional model configuration (tail 10) in figure 31. The directional stability of the conventional model became negative above $\alpha = 20^\circ$, whereas the stability of both three-body configurations showed only small reductions at high angles of attack.

The contribution of the vertical tail at any angle of attack, expressed as a fraction of the contribution at $\alpha = 0^\circ$, is compared for several model arrangements in figure 32. It is of interest to note that although the tail contributions for the three-body model appeared to be better than that of the conventional model above an angle of attack of 25°, the contributions for the three-body model were invariably smaller than for the conventional model at lower angles. It thus may be concluded that the improved directional stability of the complete three-body configurations, as mentioned in the preceding paragraph, over that of the conventional model configuration is not due to the vertical-tail contribution but is caused by the stability characteristics of the wing-fuselage configuration.

CONCLUSIONS

Results of a low-speed investigation of the static longitudinal and lateral stability characteristics of an airplane model with three bodies and of a conventional (single-fuselage) model indicate the following conclusions:

1. The pitching-moment characteristics for the three-body model appear to bear about the same relation to height of the horizontal tail as that which has been well established by previous investigations of conventional (single-fuselage) configurations. It appears that satisfactory longitudinal stability can be obtained with several different arrangements of horizontal tails located in or near the wing-chord plane for the three-body model.

2. All the tail-on configurations of the three-body model were directionally stable throughout the angle-of-attack range and were greatly improved over the conventional model configuration which was directionally unstable above an angle of attack of 20°. The improved directional stability for the complete three-body model results from the fact that with tail off, the directional stability becomes positive at high angles of attack.

Langley Research Center,
National Aeronautics and Space Administration,
Langley Field, Va., December 12, 1956.

REFERENCES

1. Polhamus, Edward C., and Hallissy, Joseph M., Jr.: Effect of Airplane Configuration on Static Stability at Subsonic and Transonic Speeds. NACA RM L56A09a, 1956.

2. Zimmerman, Charles H.: Recent Stability and Aerodynamic Problems and Their Implications as to Load Estimation. NACA RM L55E11a, 1955.

3. Edwards, George G., and Savage, Howard F.: A Horizontal-Tail Arrangement for Counteracting Static Longitudinal Instability of Sweptback Wings. NACA RM A56D06, 1956.

4. Goodson, Kenneth W., and Becht, Robert E.: Wind-Tunnel Investigation at High Subsonic Speeds of the Static Longitudinal Stability Characteristics of a Complete Model Having Cropped-Delta, Swept, and Unswept Wings and Several Horizontal-Tail Heights. NACA RM L54H12, 1954.

5. Polhamus, Edward C., and Spreemann, Kenneth P.: Subsonic Wind-Tunnel Investigation of the Effect of Fuselage Afterbody on Directional Stability of Wing-Fuselage Combinations at High Angles of Attack. NACA TN 3896, 1956.

TABLE I.- SINGLE-FUSELAGE ORDINATES

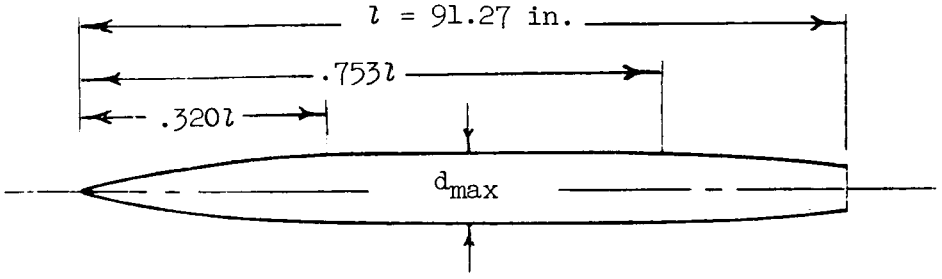

Ordinates, percent length	
Station	Radius
0	0
3.28	.91
6.57	1.71
9.86	2.41
13.15	3.00
16.43	3.50
19.72	3.90
23.01	4.21
26.29	4.43
29.58	4.53
32.00	4.57
75.34	4.57
76.69	4.54
79.98	4.38
83.26	4.18
86.55	3.95
89.84	3.72
93.13	3.49
96.41	3.26
100.00	3.02

TABLE II.- THREE-BODY ORDINATES

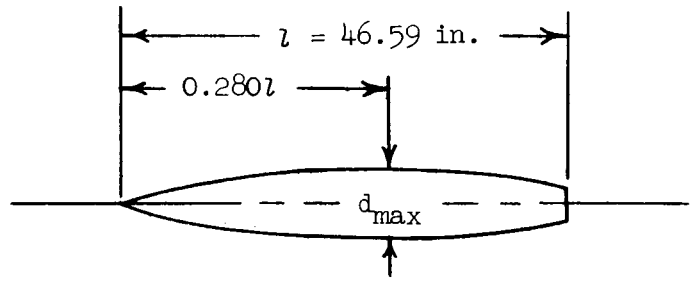

Ordinates, percent length	
Station	Radius
0	0
.60	.44
.90	.56
1.50	.81
3.00	1.36
6.00	2.28
9.00	3.05
12.00	3.72
18.00	4.90
24.00	5.84
30.00	6.55
36.00	7.07
42.00	7.43
48.00	7.67
54.00	7.83
60.00	7.87
66.00	7.80
72.00	7.60
78.00	7.26
84.00	6.73
90.00	5.91
96.00	4.77
100.00	3.94

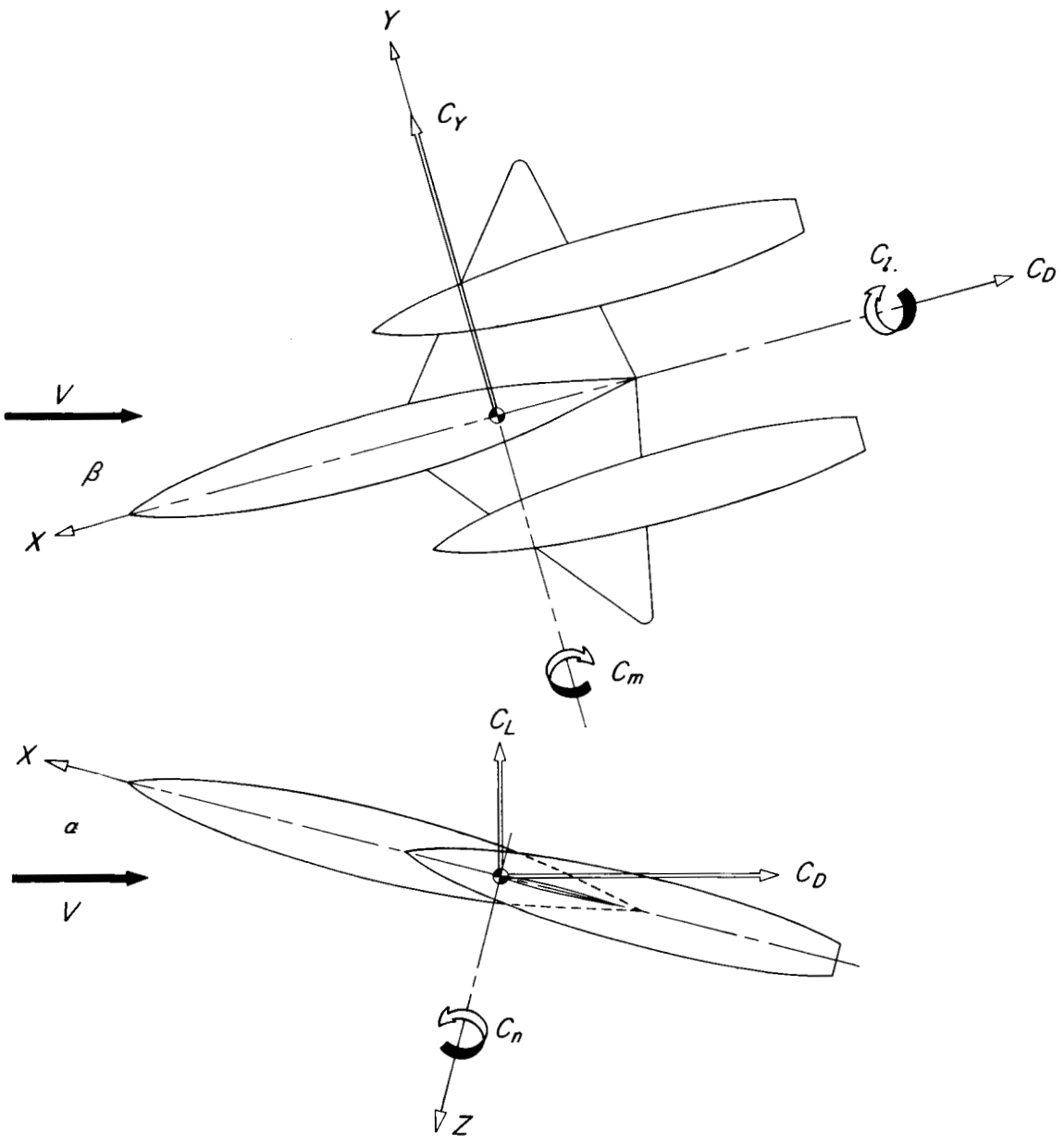

Figure 1.- Axes system and conventions used to define positive sense of forces, moments, and angles.

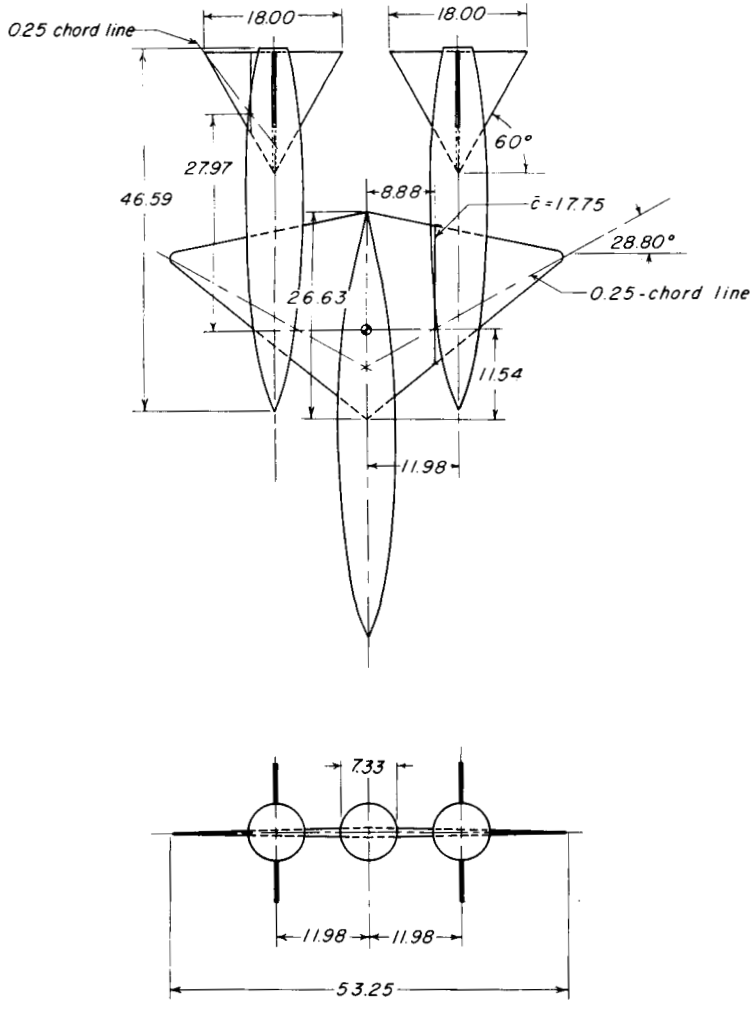

Physical Characteristics

Wing	
Sweep of $c/4$, deg	28.80
Area, sq ft	4.92
Span (theoretical)	53.25
Aspect ratio	4
Taper ratio	0
Mean aerodynamic chord, ft	1.48
Airfoil section parallel to plane of symmetry	NACA 65A004
Horizontal tails (each)	
Area, sq ft	.97
Aspect ratio	2.31
Airfoil section (flat plate)	
Vertical tails (each)	
Area, sq ft	.97
Aspect ratio	2.31
Airfoil section (flat plate)	

0 5 10
Scale, inches

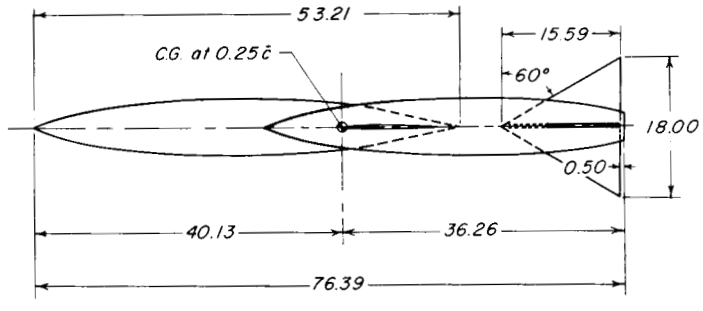

(a) Three-body model.

Figure 2.- Drawing of models employed. All dimensions are in inches.

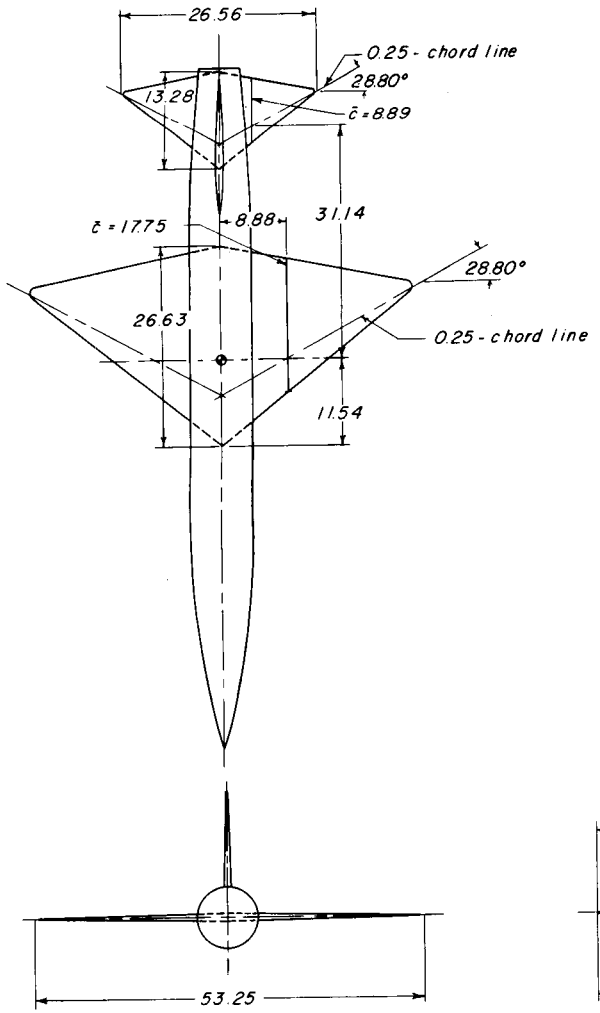

Physical Characteristics

Wing	
Sweep of $c/4$, deg	28.80
Area, sq ft	4.92
Span (theoretical)	53.25
Aspect ratio	4
Taper ratio	0
Mean aerodynamic chord, ft	1.48
Airfoil section parallel to plane of symmetry	NACA 65A004
Horizontal tail	
Area, sq ft	1.22
Aspect ratio	4
Airfoil section (flat plate)	
Vertical tail	
Area, sq ft	1.68
Aspect ratio	1.16
Airfoil section parallel to plane of symmetry	NACA 63A009

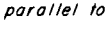

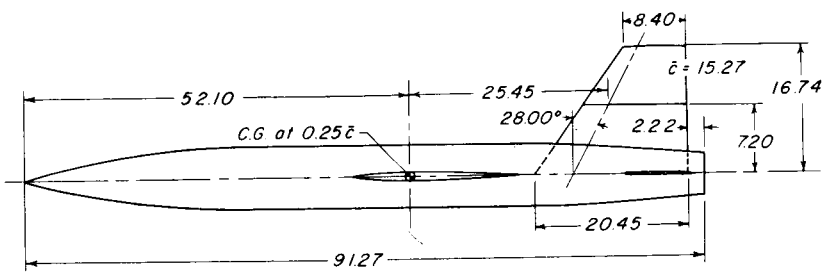

(b) Conventional model.

Figure 2.- Continued.

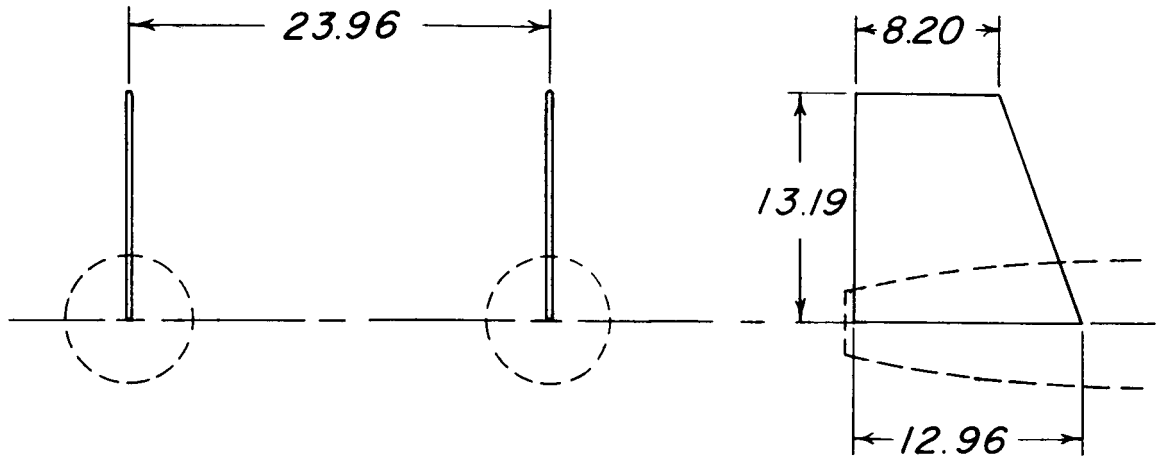

(c) Dimensions of tail assembly 5.

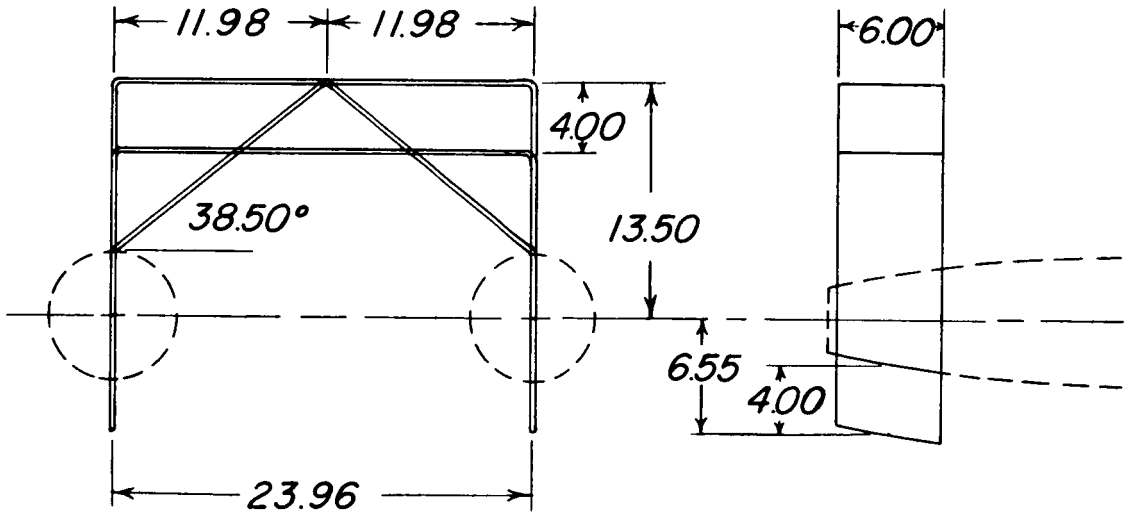

(d) Composite dimensions of tail assemblies 6 to 9.

Figure 2.- Concluded.

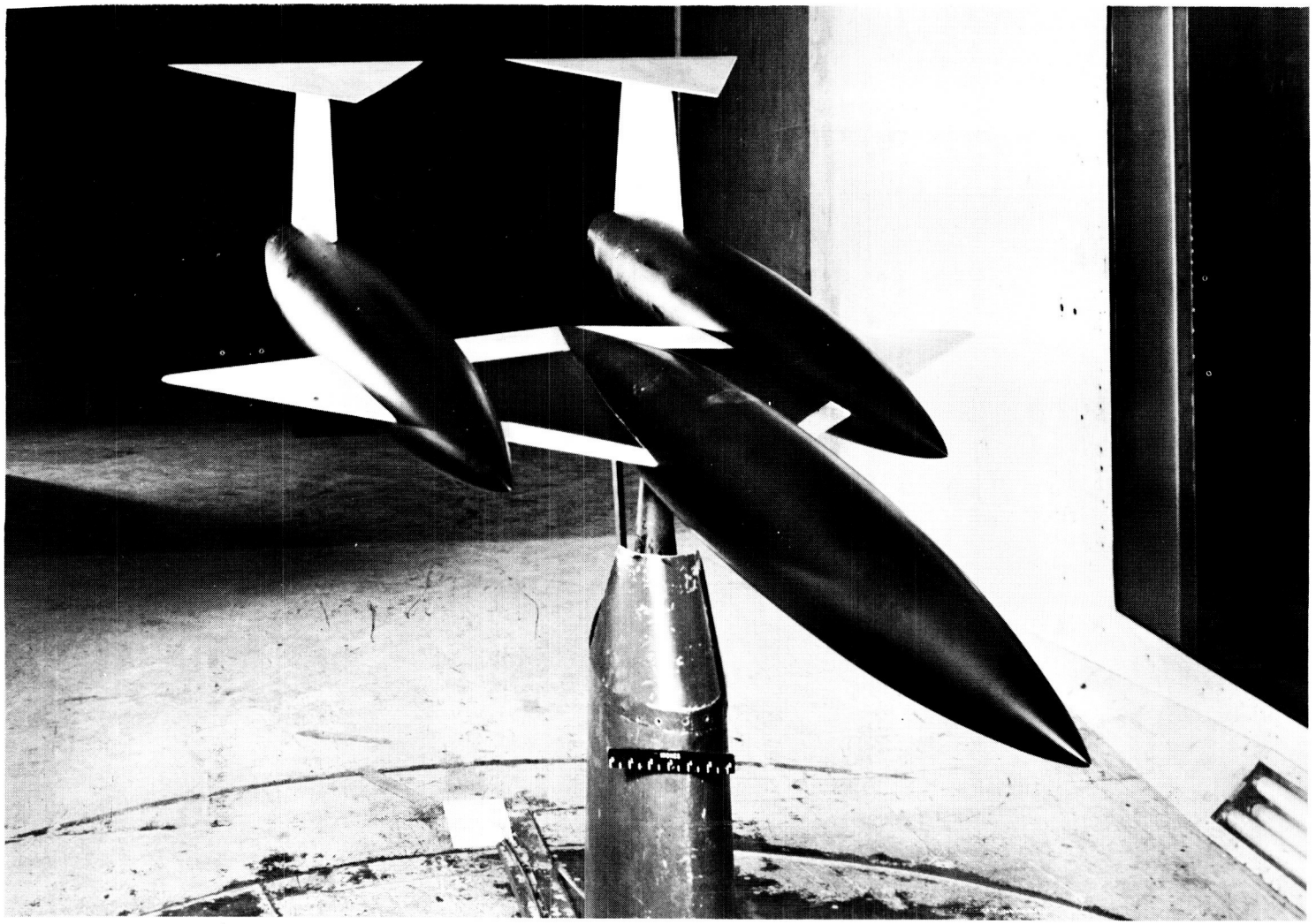

Figure 3.- Photograph of three-body model with T-tail, mounted on support strut. L-90721

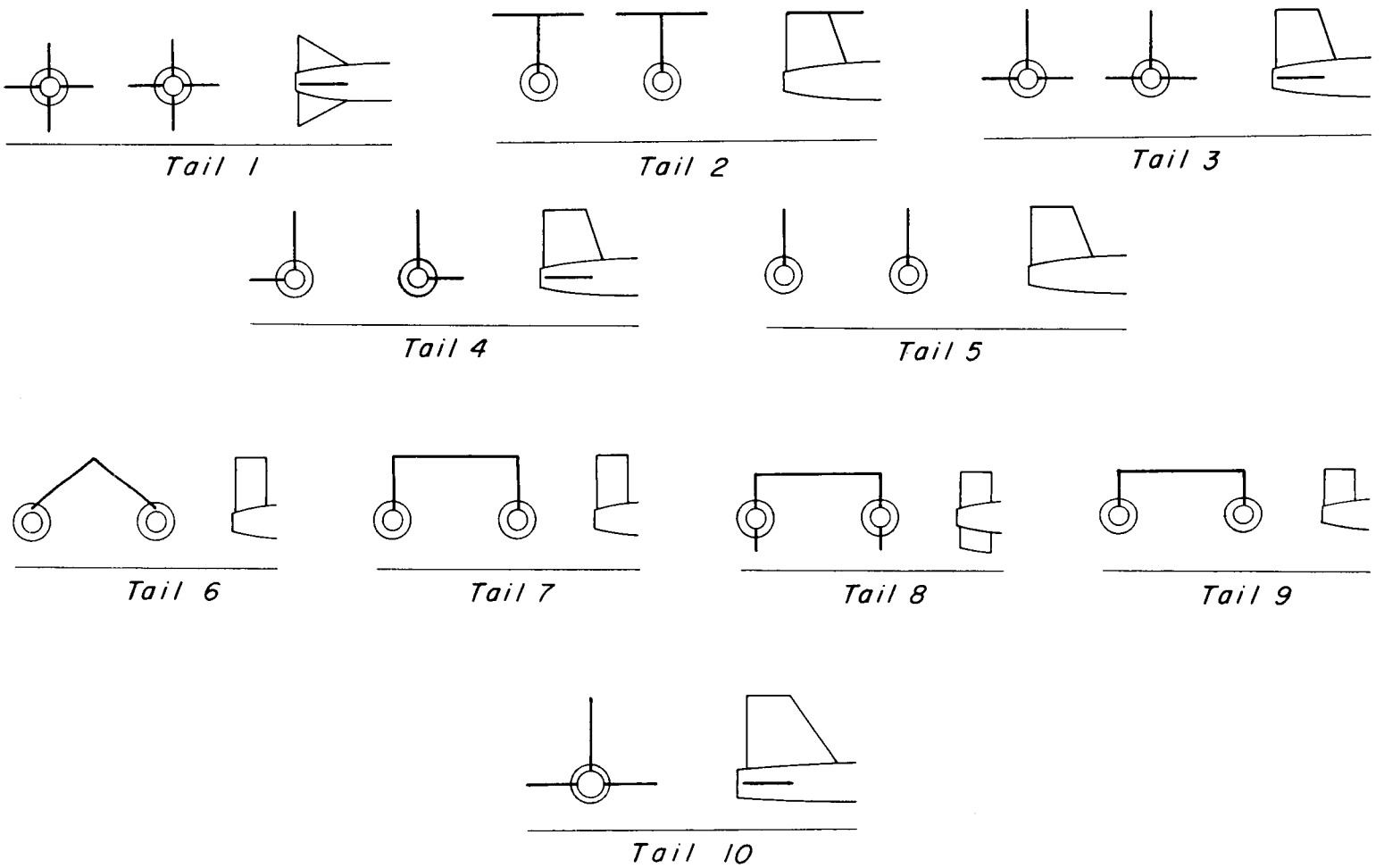

Figure 4.- Sketches of different tail arrangements.

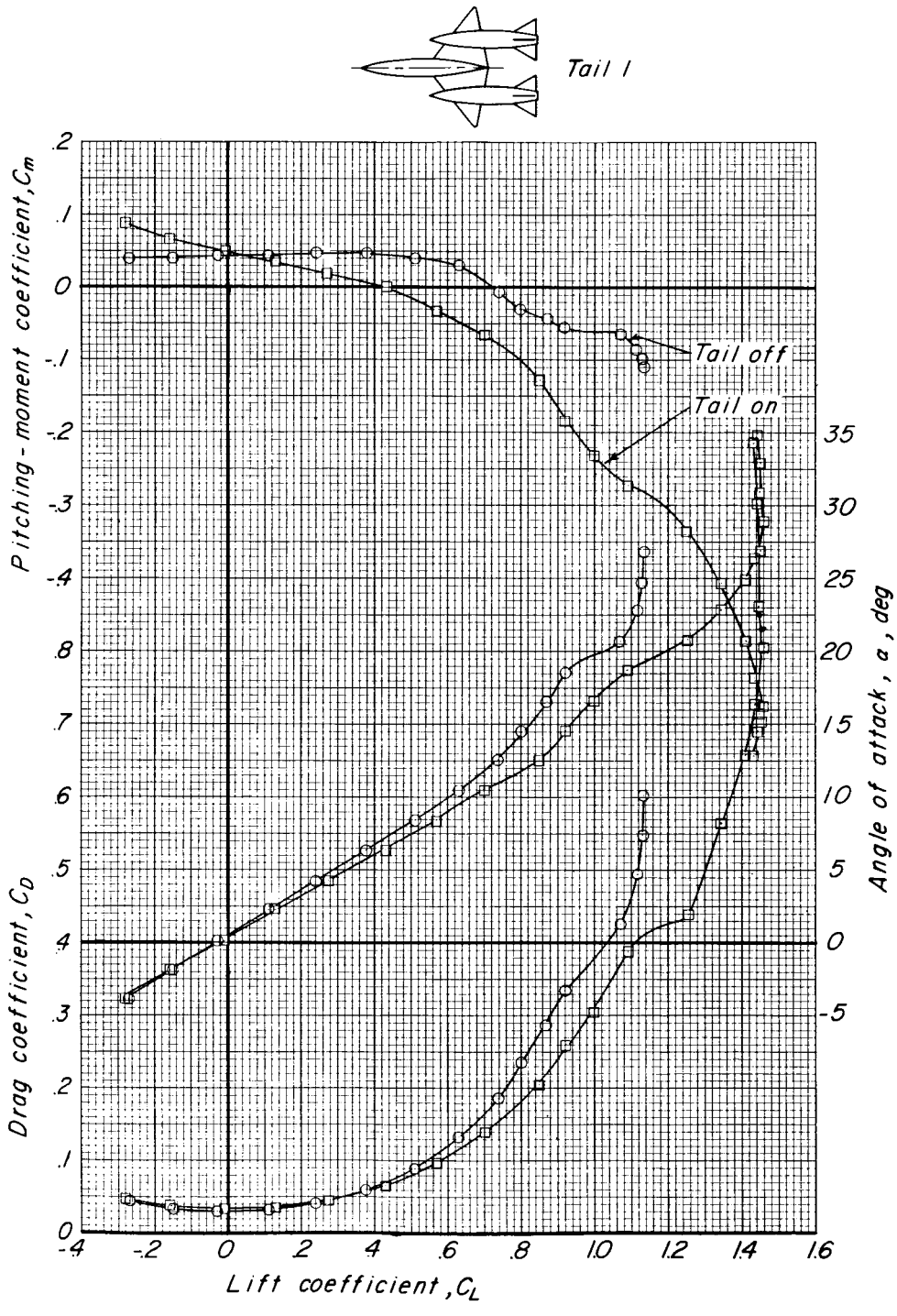

Figure 5.- Longitudinal characteristics of three-body model with tail off and with tail 1. (Results for tail 1 may apply to tail 3.)

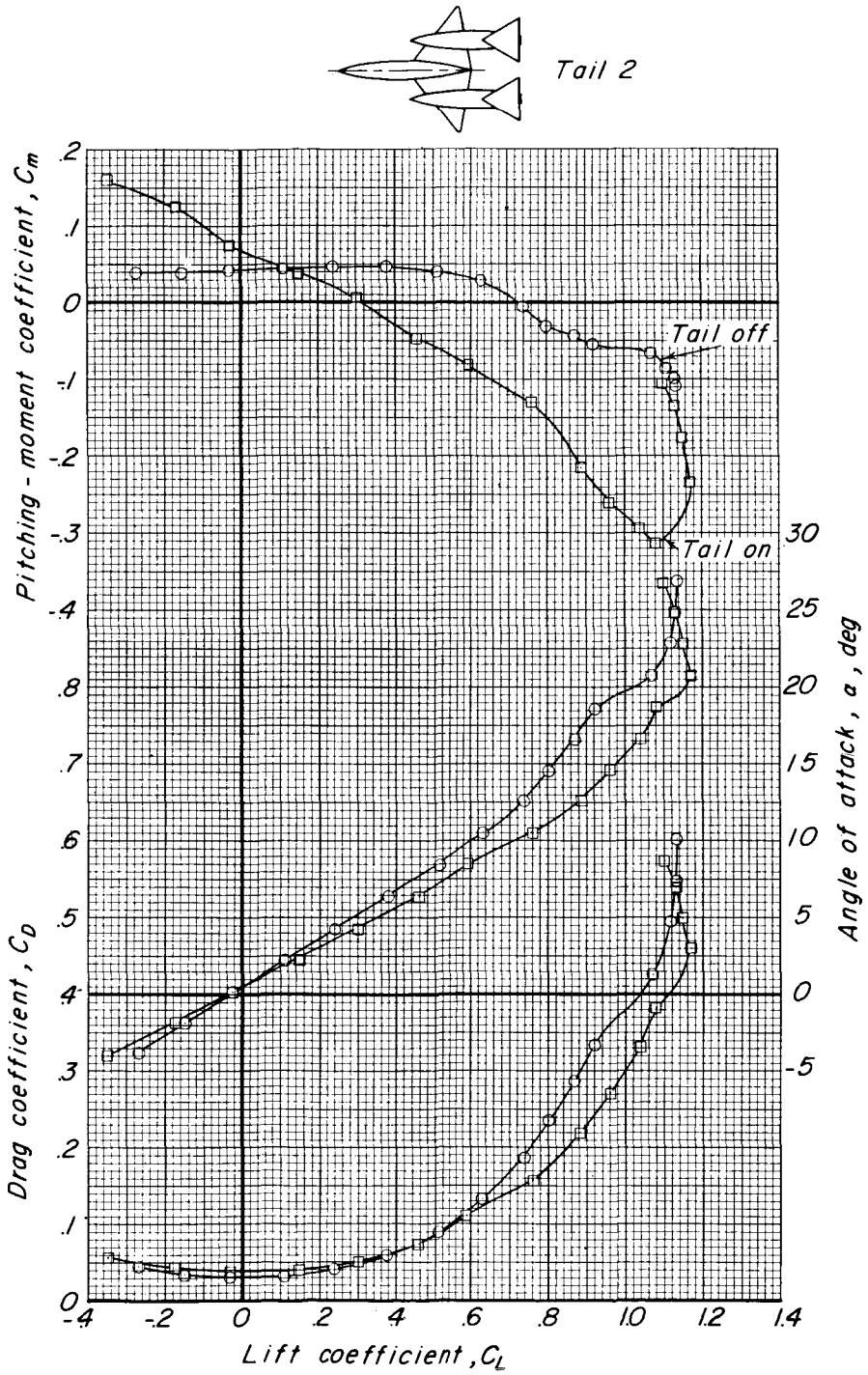

Figure 6.- Longitudinal characteristics of three-body model with tail off and with tail 2.

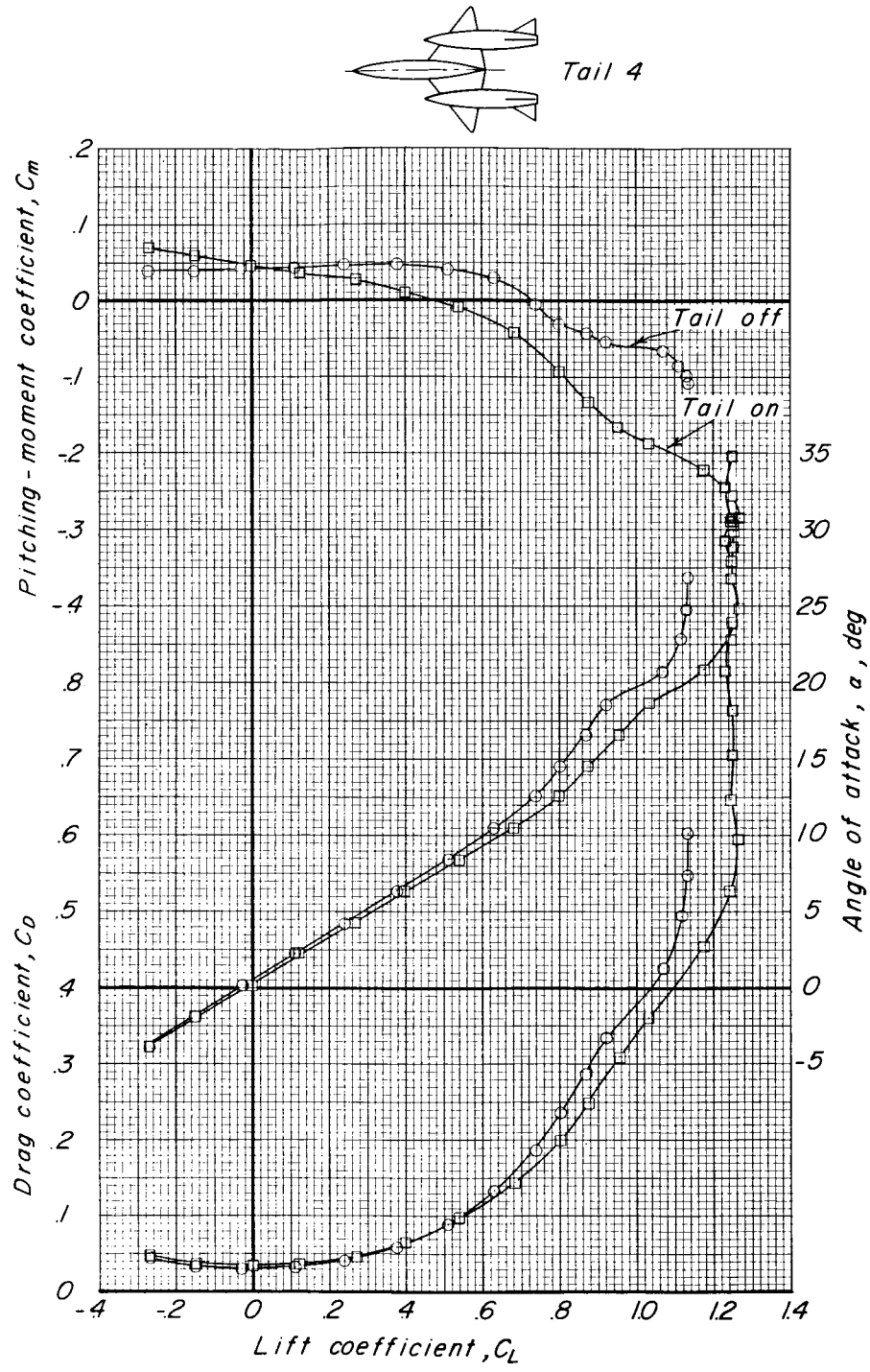

Figure 7.- Longitudinal characteristics of three-body model with tail off and with tail 4.

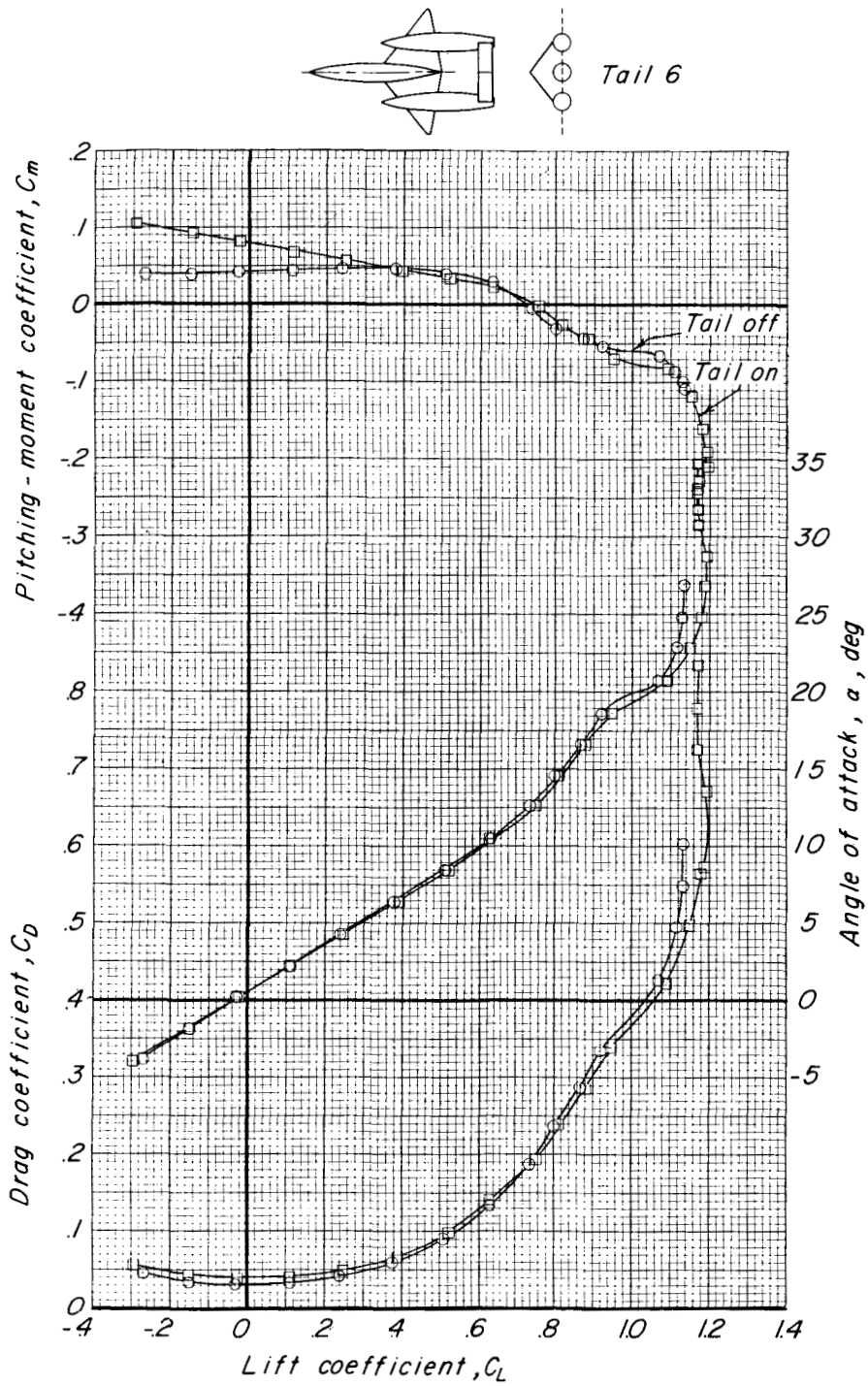

Figure 8.- Longitudinal characteristics of three-body model with tail off and with tail 6.

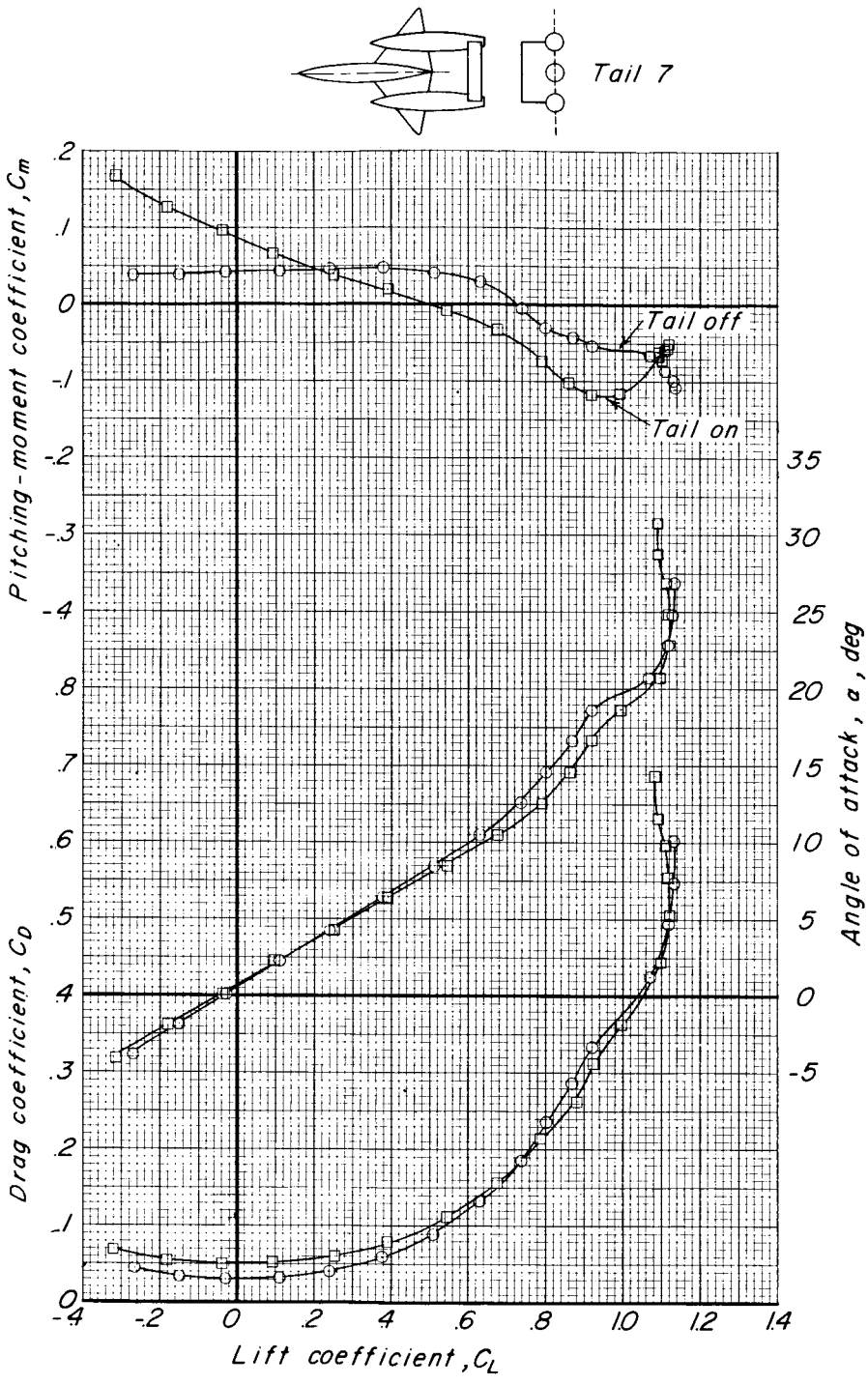

Figure 9.- Longitudinal characteristics of three-body model with tail off and with tail 7.

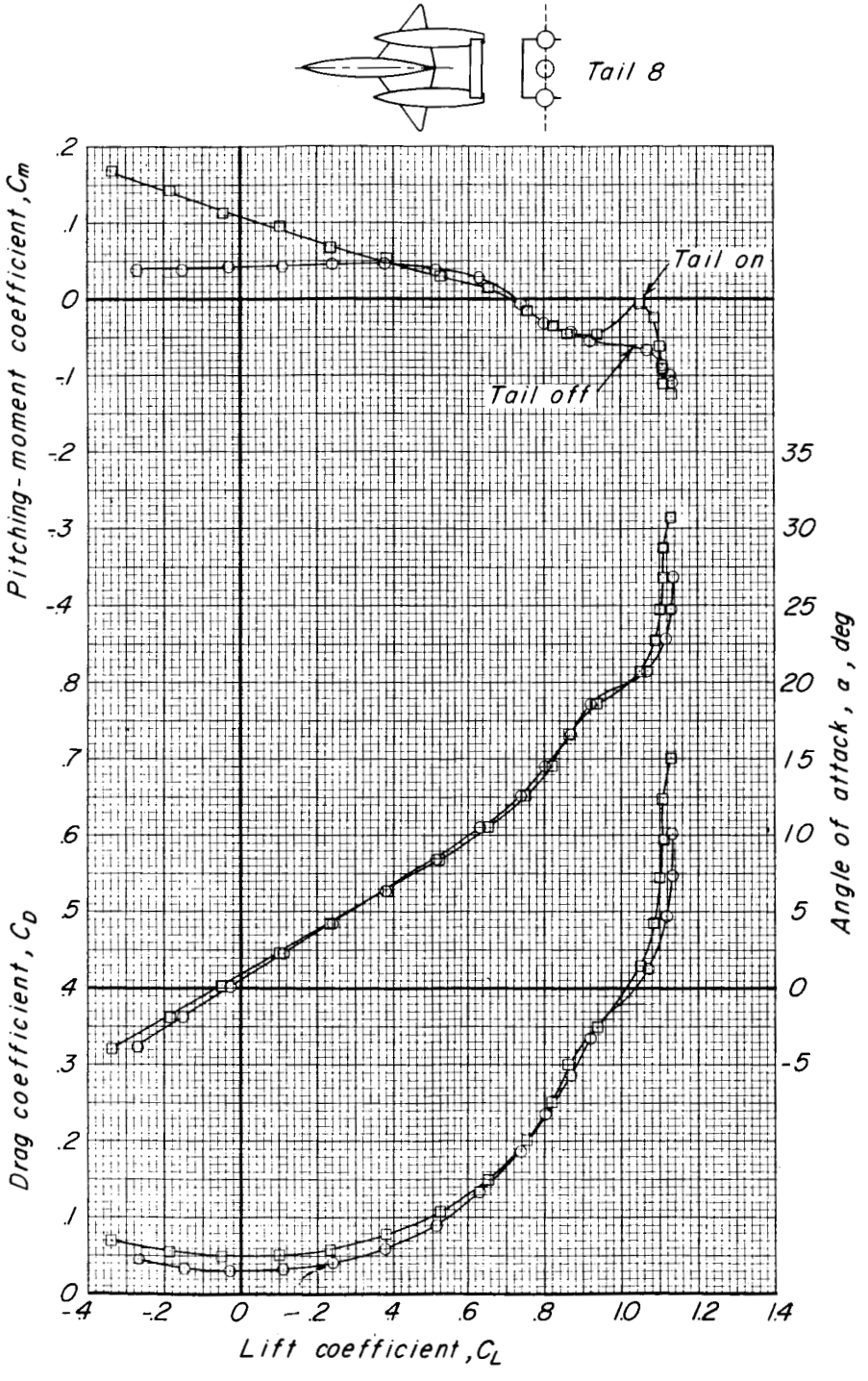

Figure 10.- Longitudinal characteristics of three-body model with tail off and with tail 8. (Results for tail 8 may apply to tail 9.)

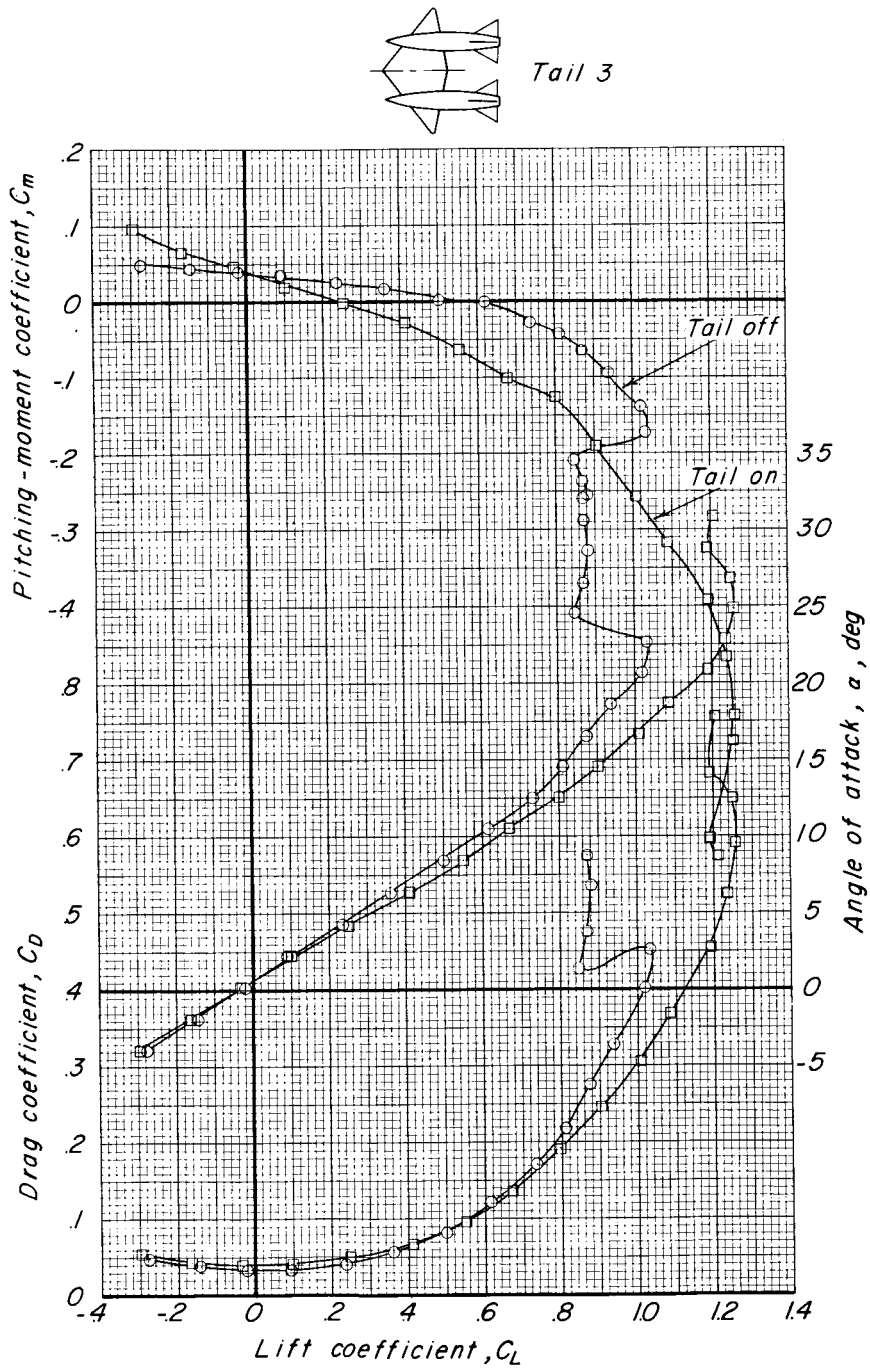

Figure 11.- Longitudinal characteristics of three-body model without center body with tail off and with tail 3. (Results for tail 3 may apply to tail 1.)

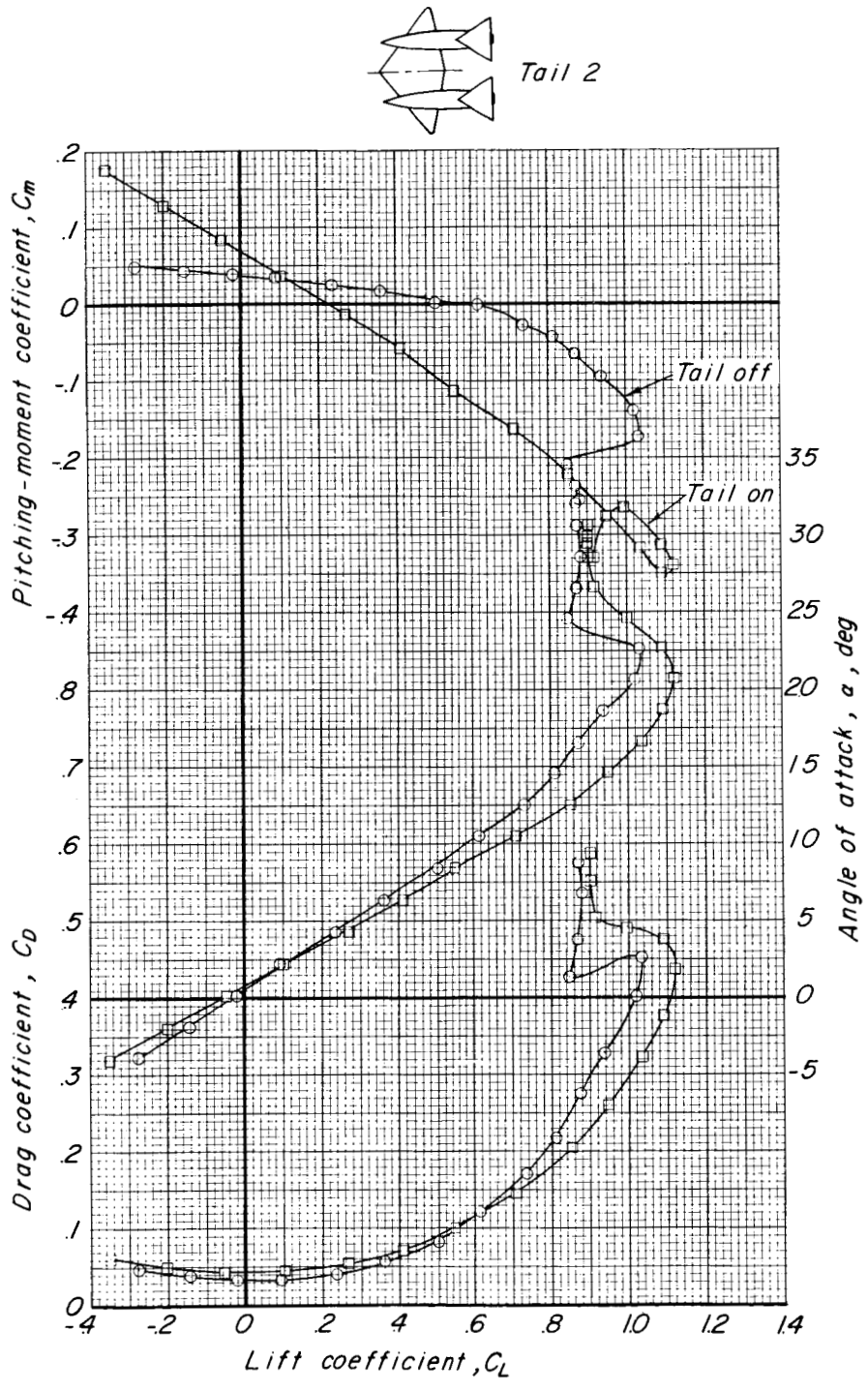

Figure 12.- Longitudinal characteristics of three-body model without center body with tail off and with tail 2.

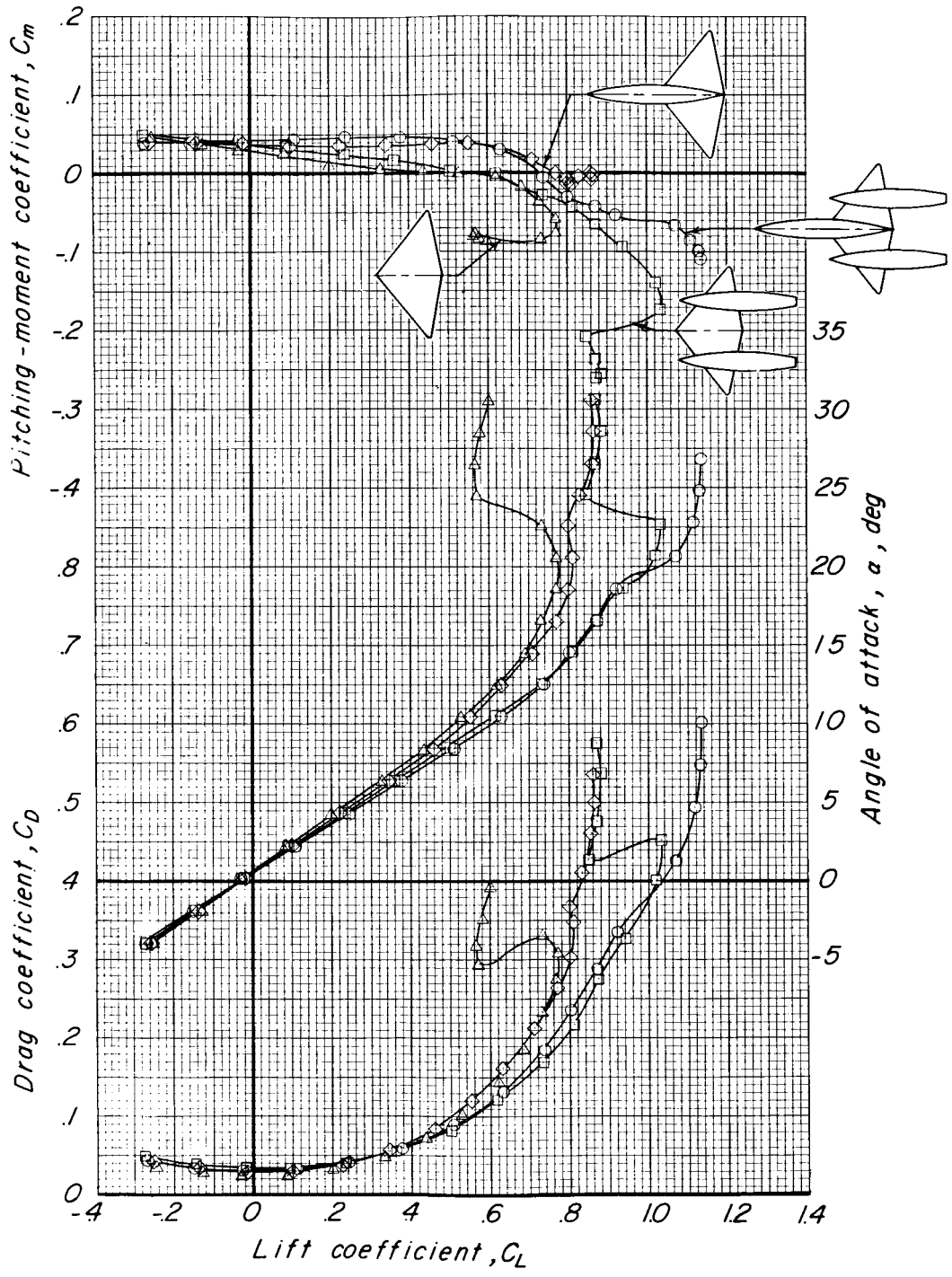

Figure 13.- Longitudinal characteristics of wing alone and in combination with one, two, or three bodies of multiple-body model.

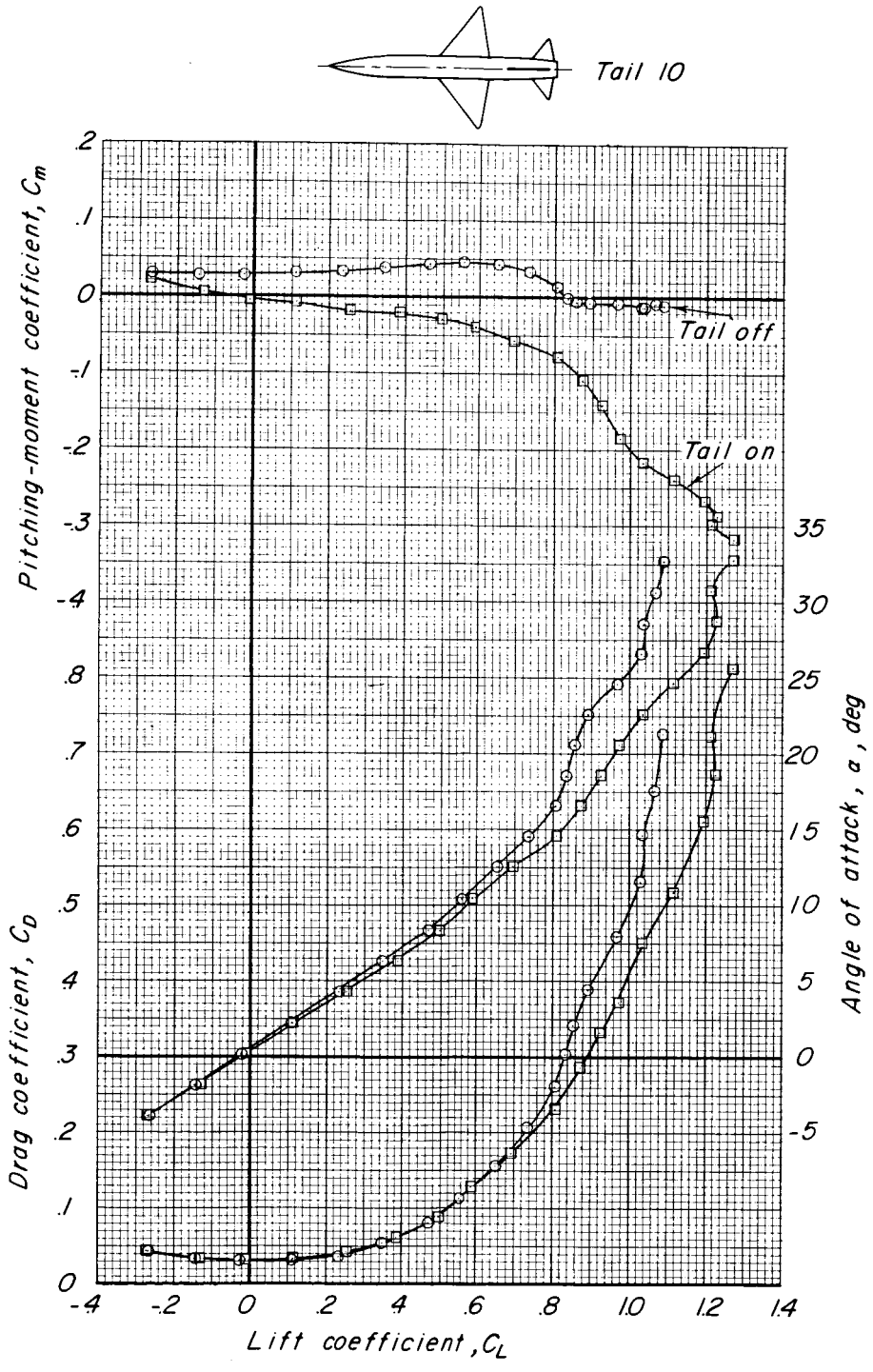

Figure 14.- Longitudinal characteristics of conventional wing-fuselage model with tail off and with tail 10.

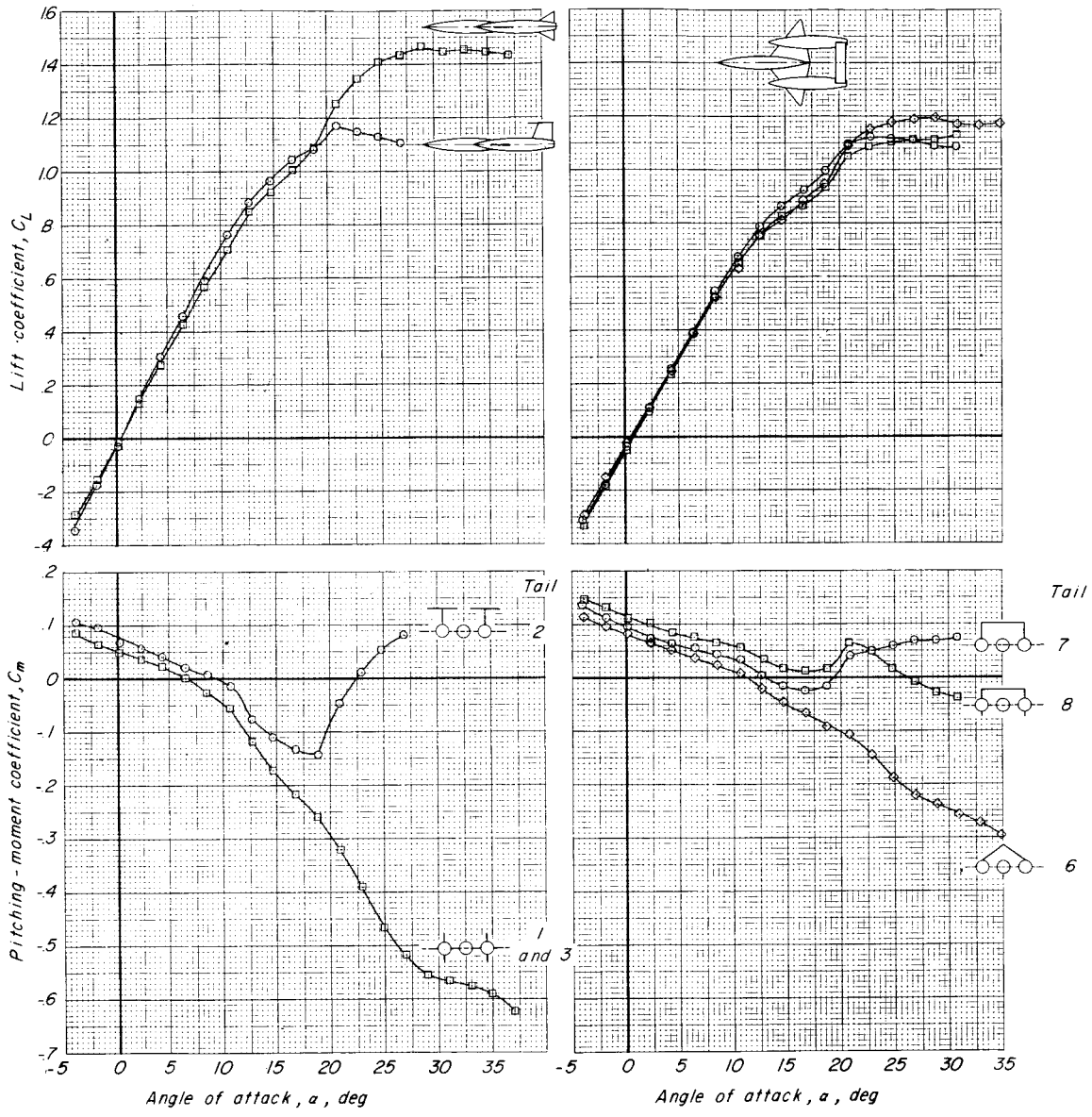

(a) Complete model with tails 1 and 2. (Results for tail 1 may apply to tail 3.)

(b) Complete model with tails 6, 7, and 8.

Figure 15.- Effect of tail and body arrangement on longitudinal characteristics.

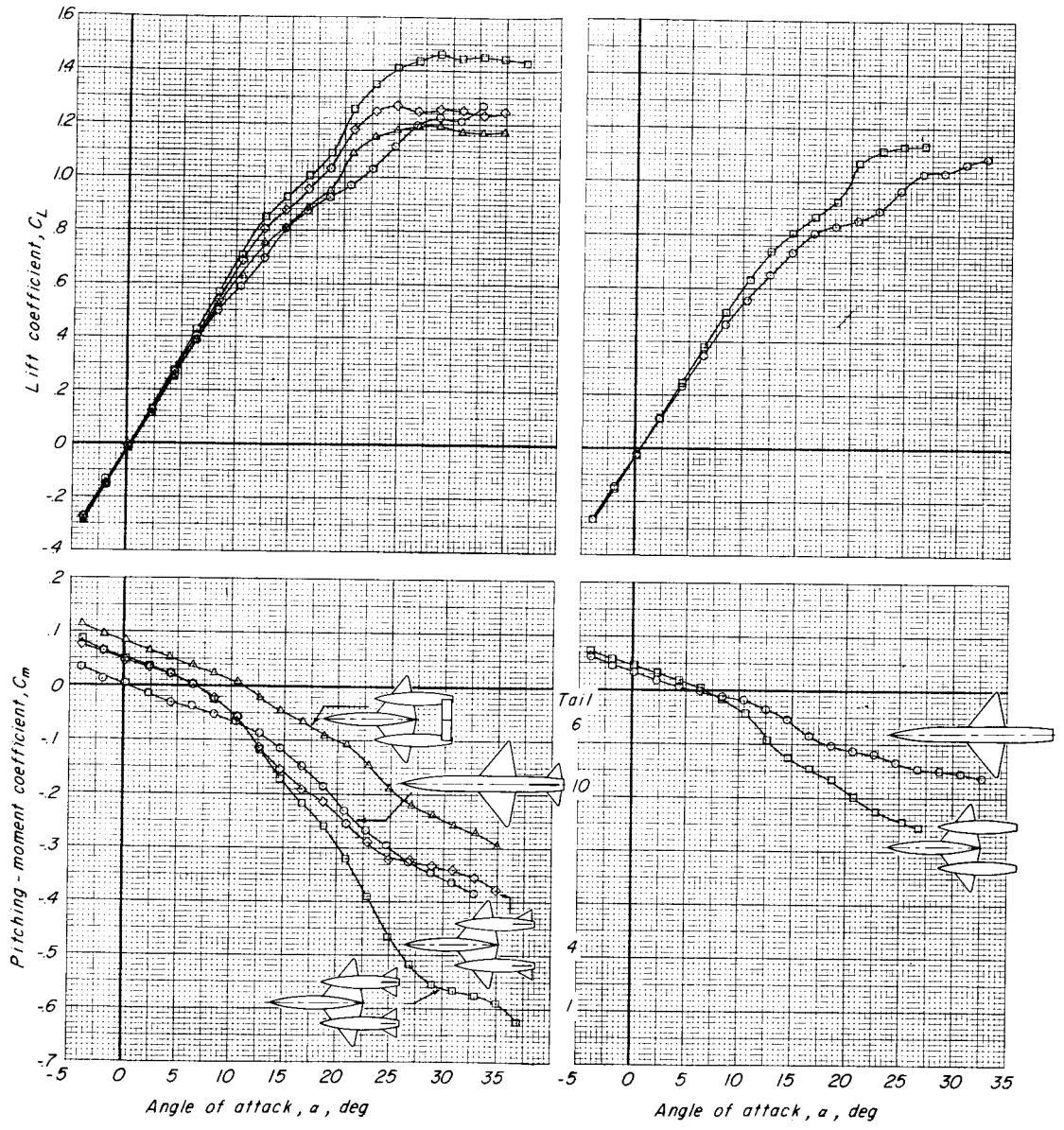

(c) Complete model with tails 1, 4, 6, and 10.

(d) Conventional model and three-body model with tail off.

Figure 15.- Concluded.

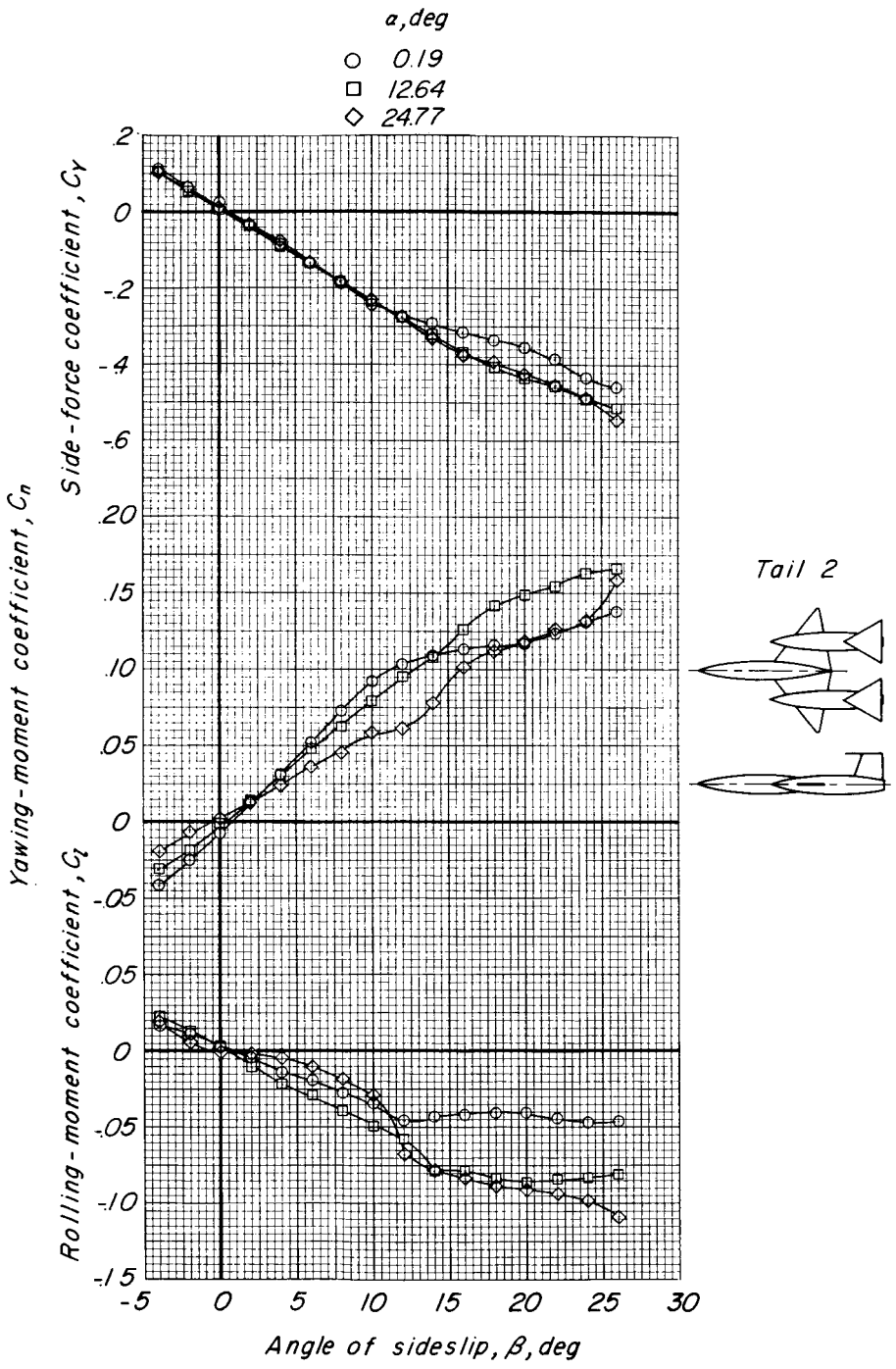

Figure 16.- Variation of static lateral aerodynamic characteristics with angle of sideslip for three-body model with tail 2 at several constant angles of attack.

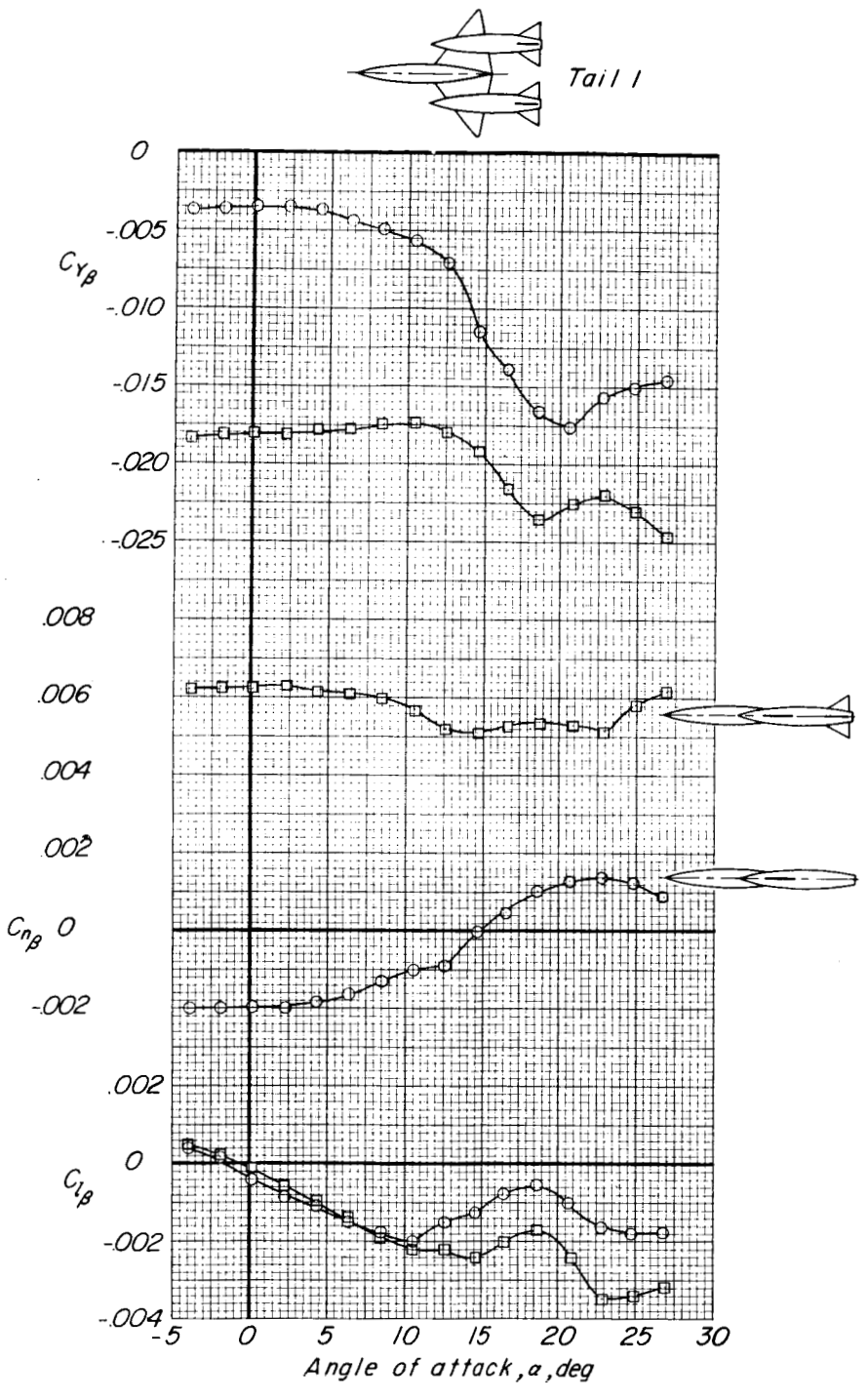

Figure 17.- Variation of static lateral stability derivatives with angle of attack for three-body model with tail off and with tail 1.

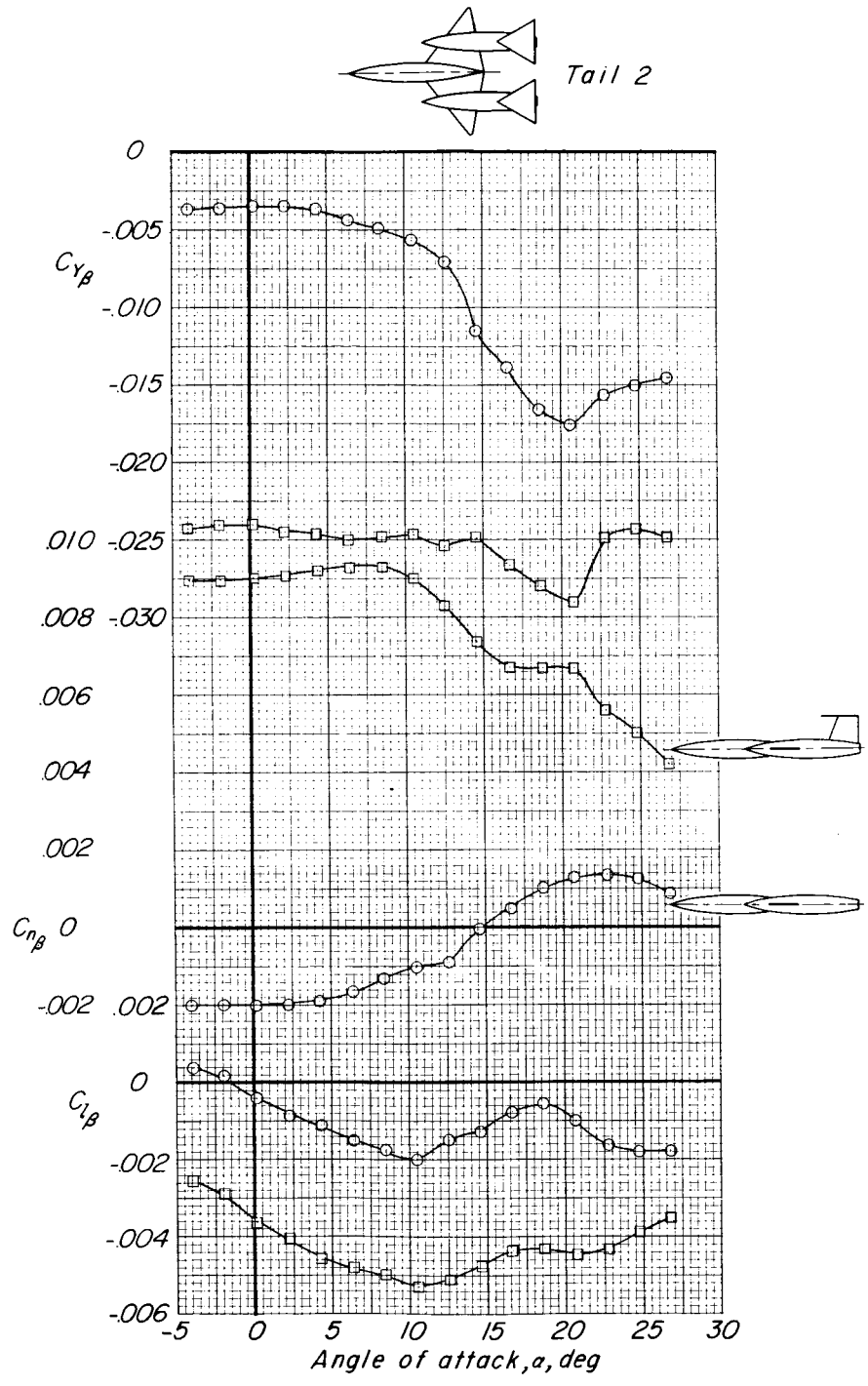

Figure 18.- Variation of static lateral stability derivatives with angle of attack for three-body model with tail off and with tail 2.

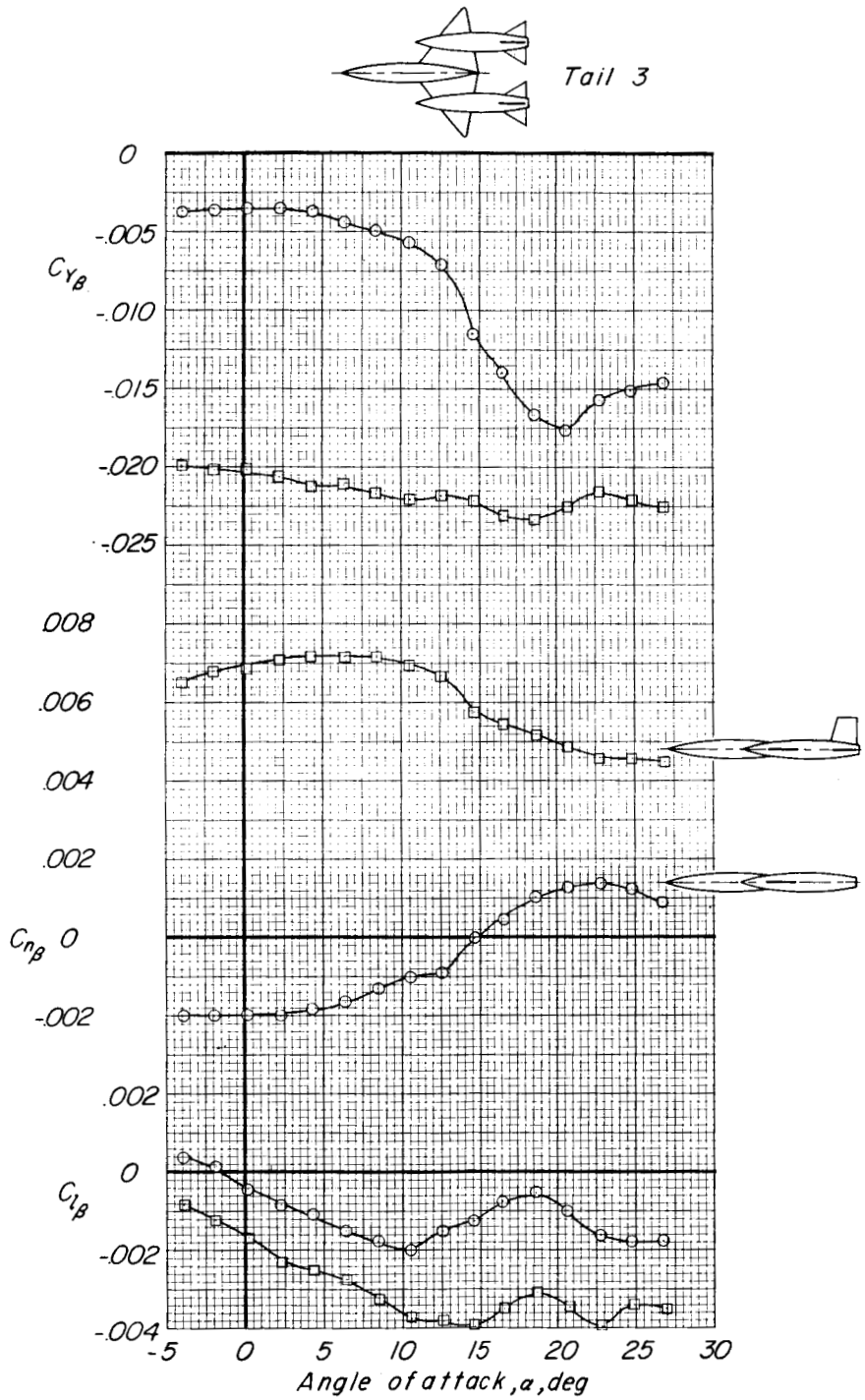

Figure 19.- Variation of static lateral stability derivatives with angle of attack for three-body model with tail off and with tail 3.

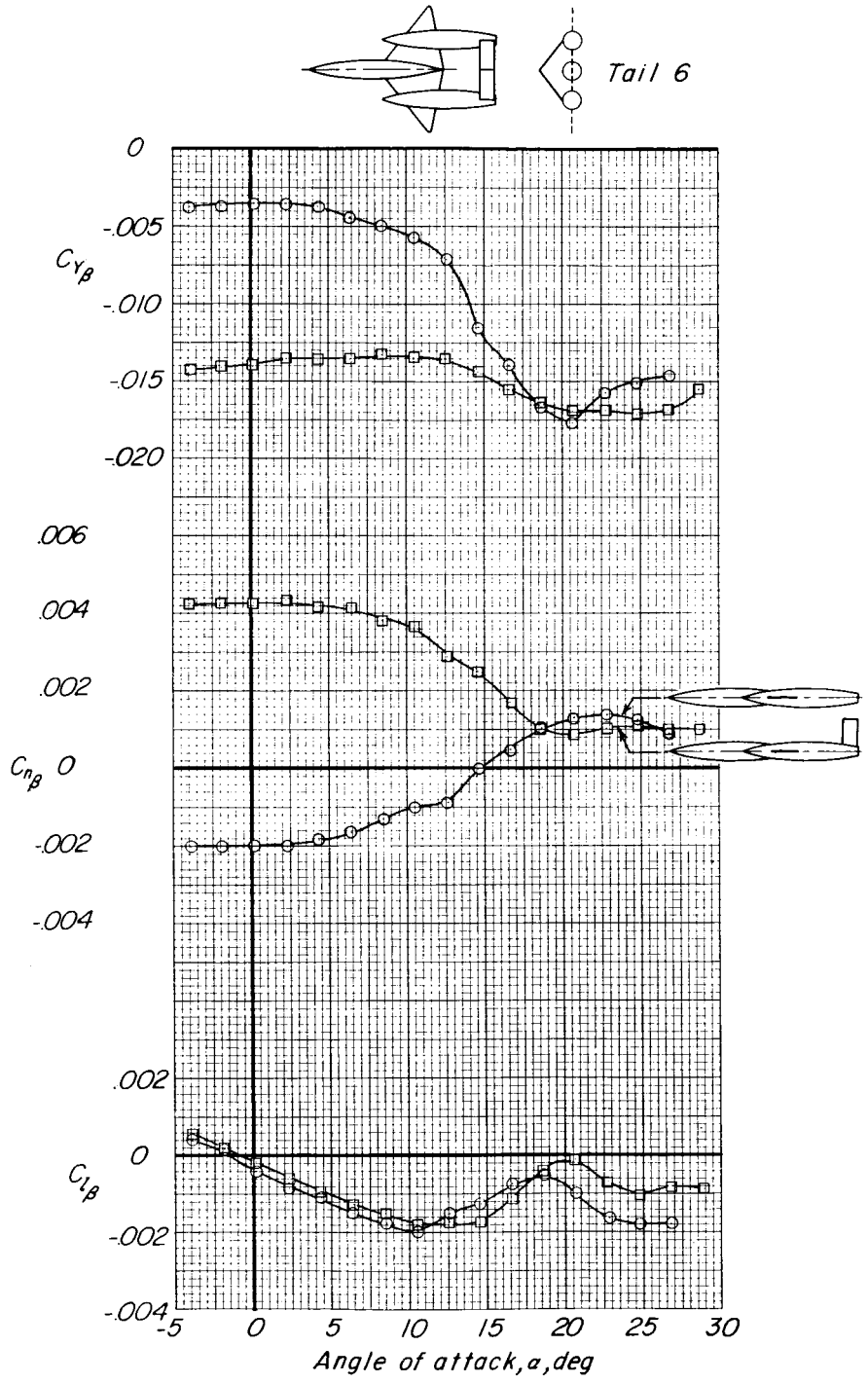

Figure 20.- Variation of static lateral stability derivatives with angle of attack for three-body model with tail off and with tail 6.

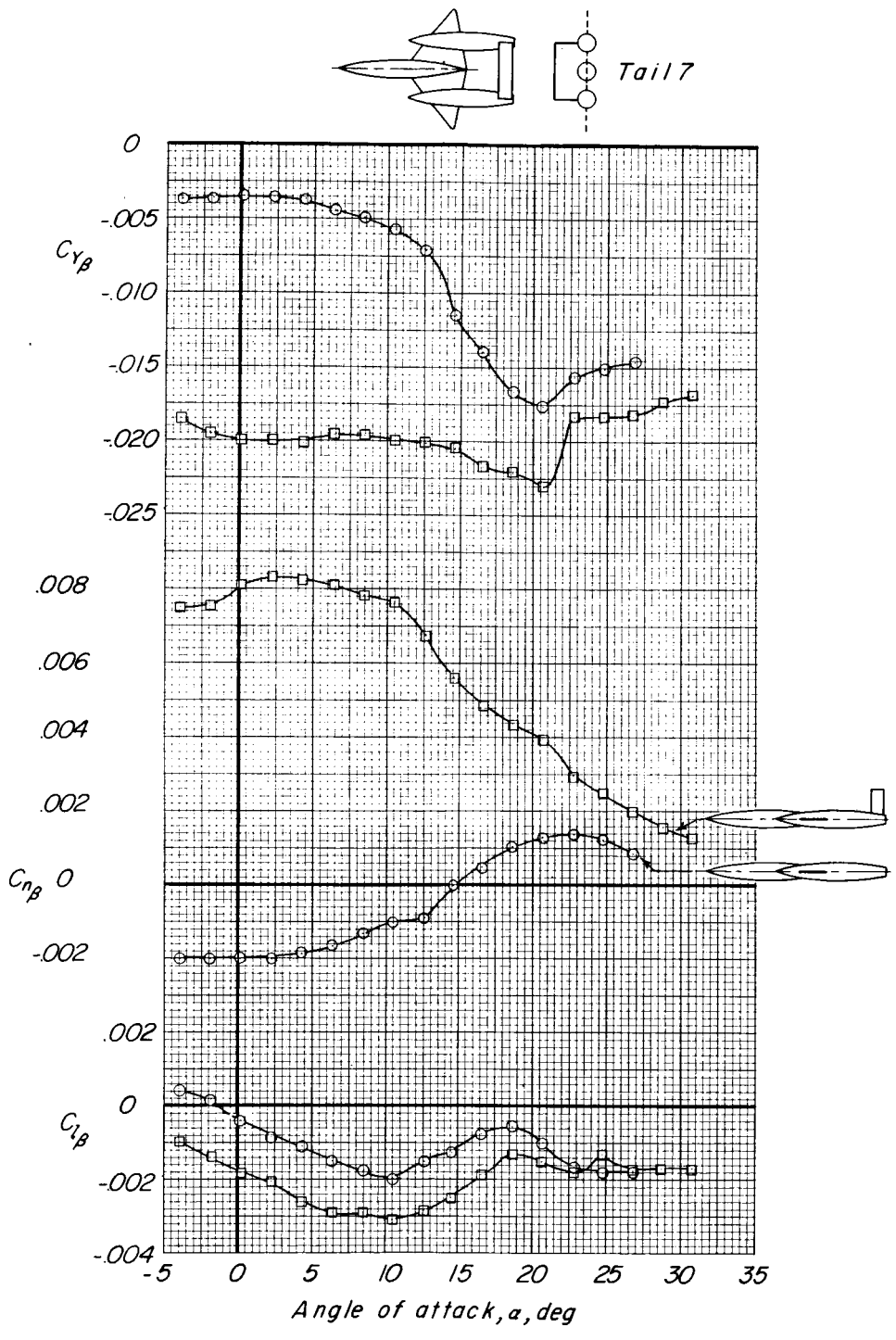

Figure 21.- Variation of static lateral stability derivatives with angle of attack for three-body model with tail off and with tail 7.

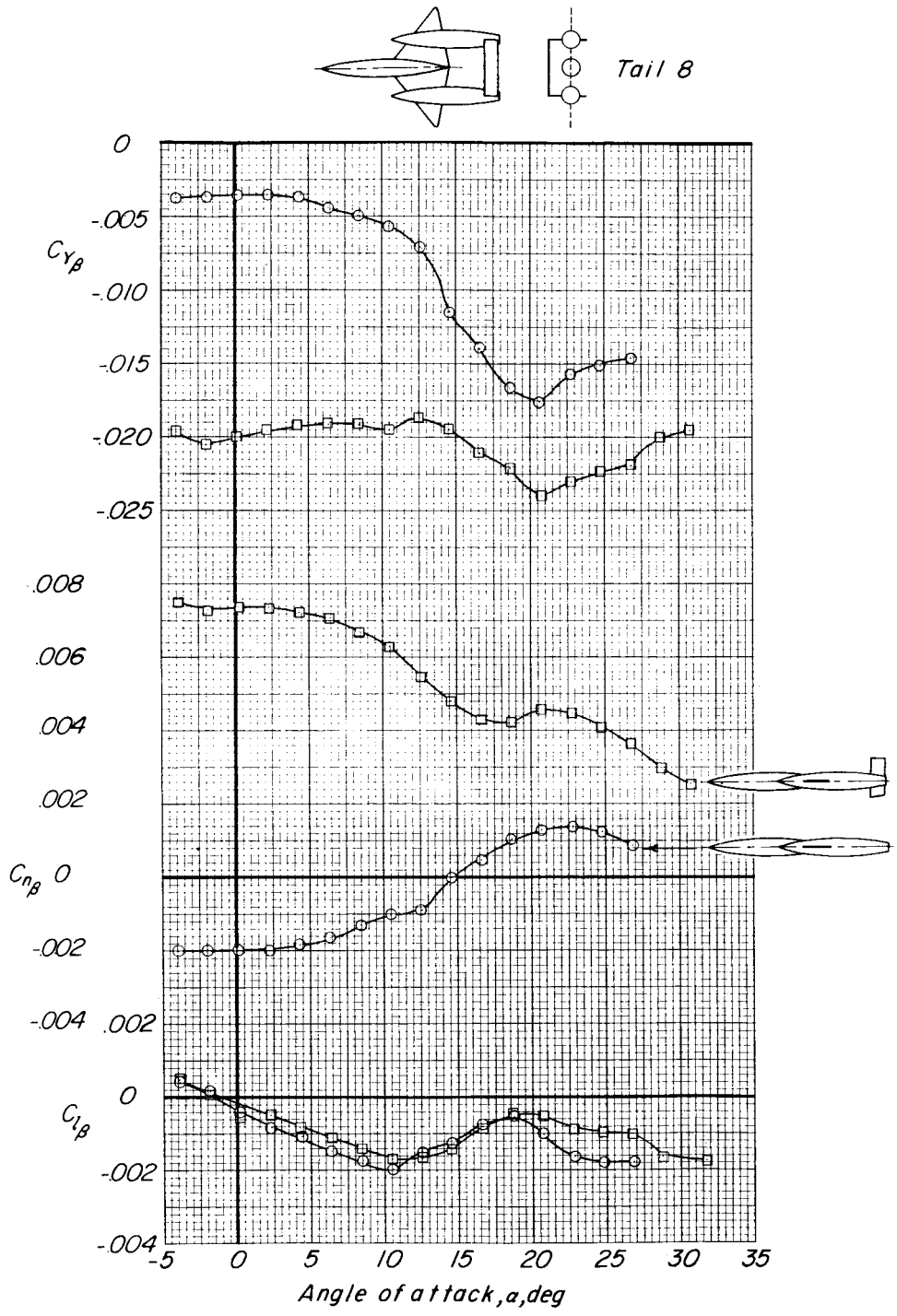

Figure 22.- Variation of static lateral stability derivatives with angle of attack for three-body model with tail off and with tail 8.

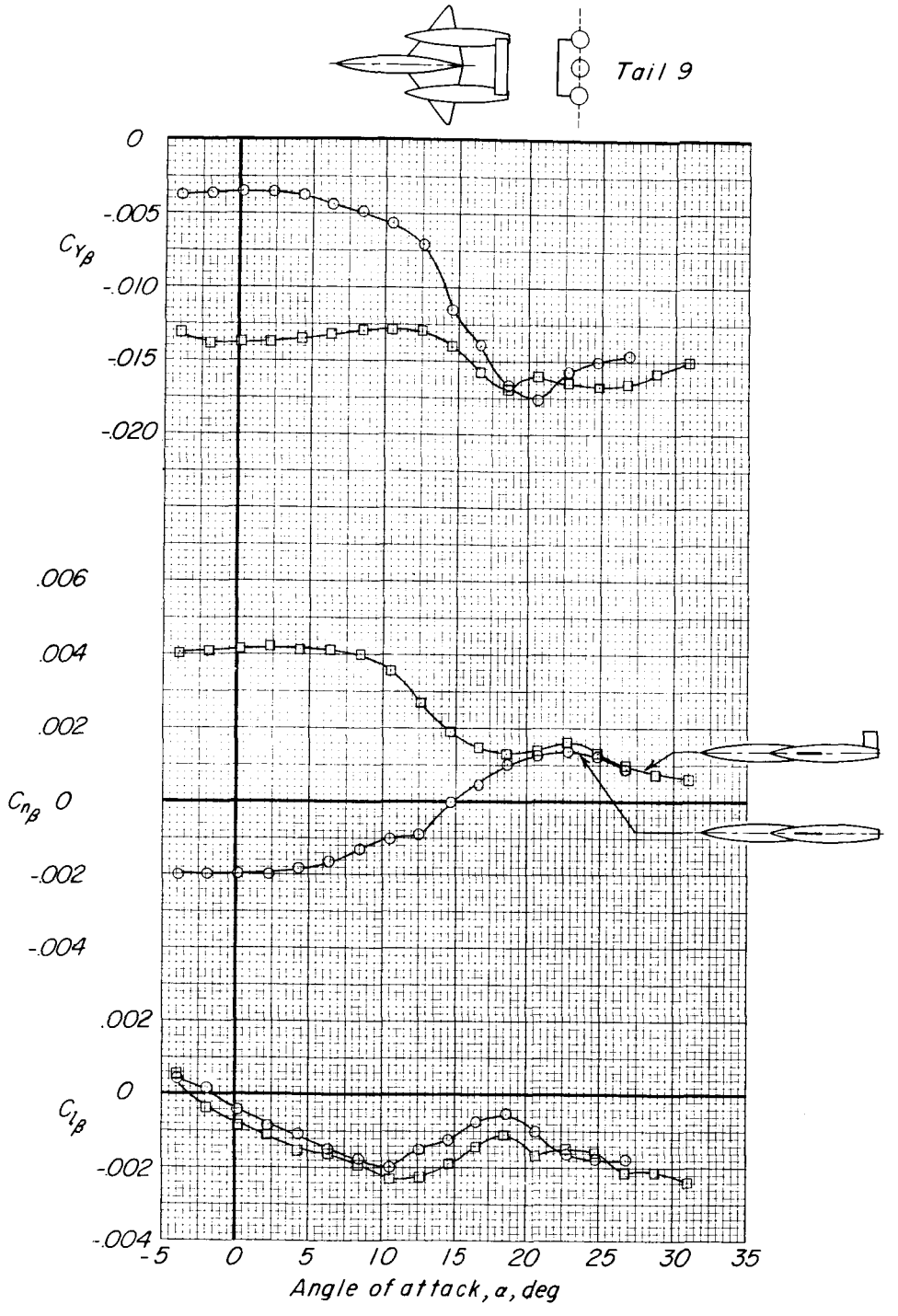

Figure 23.- Variation of static lateral stability derivatives with angle of attack for three-body model with tail off and with tail 9.

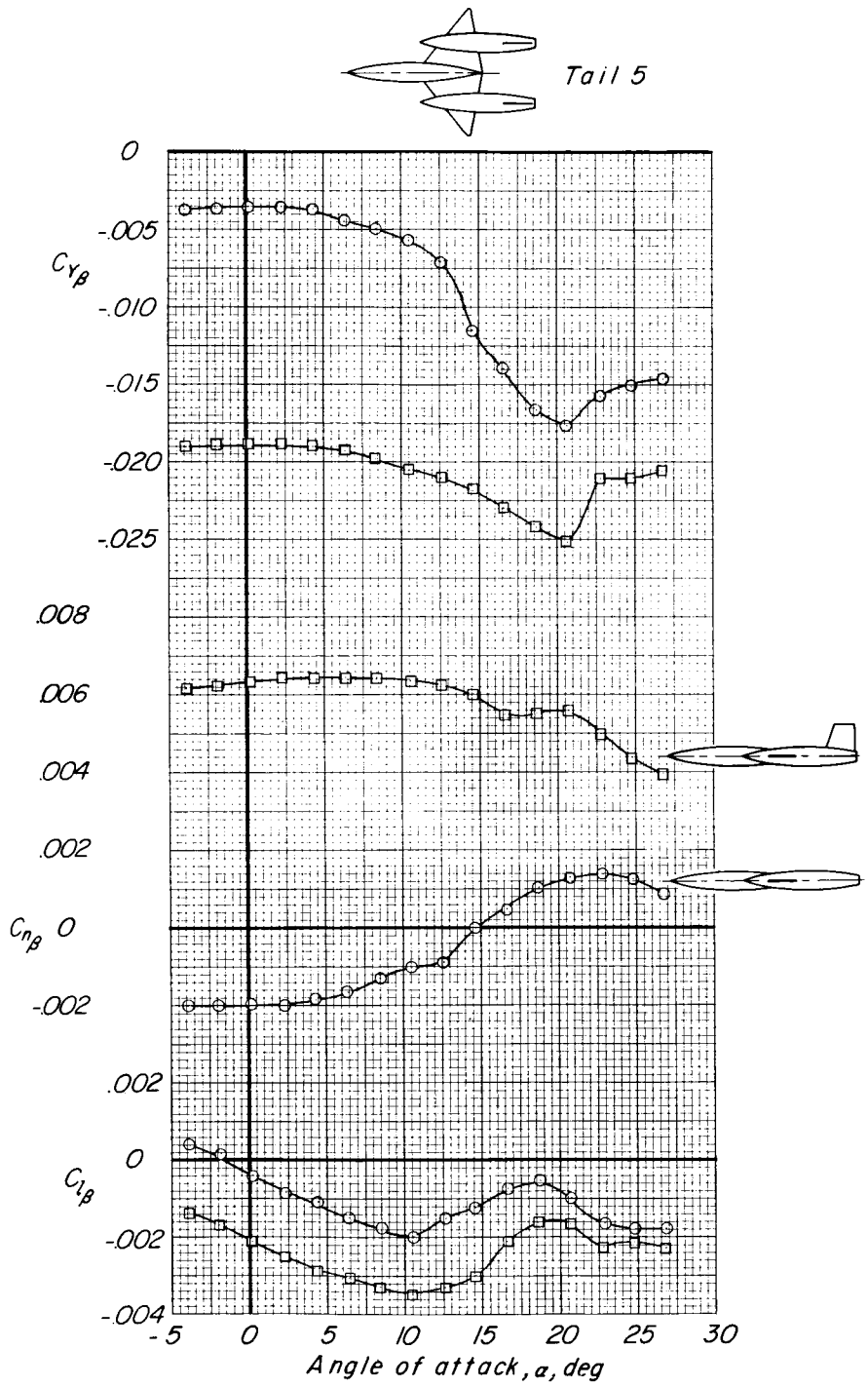

Figure 24.- Variation of static lateral stability derivatives with angle of attack for three-body model with tail off and with tail 5.

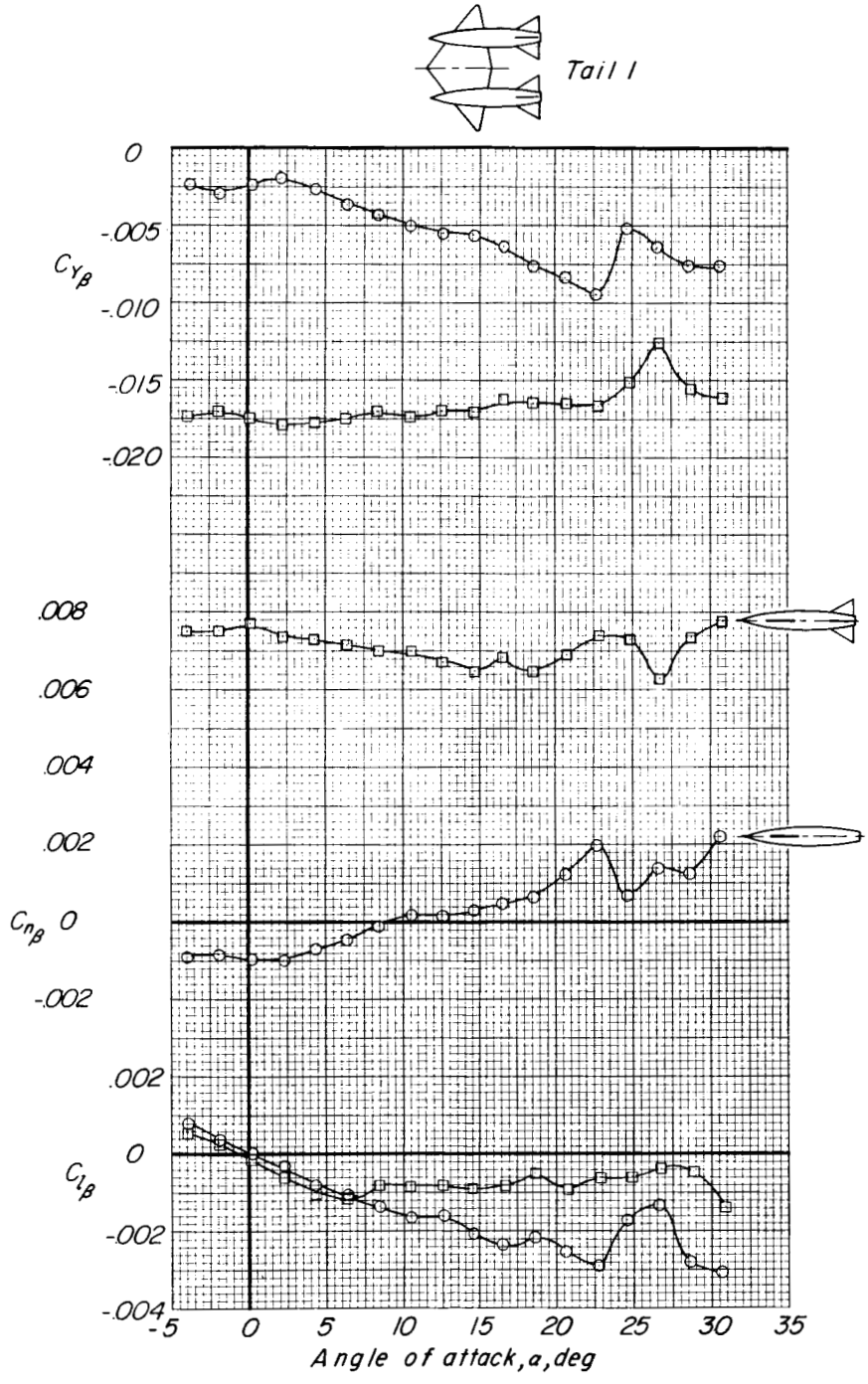

Figure 25.- Variation of static lateral stability derivatives with angle of attack for three-body model without the center body with tail off and with tail 1.

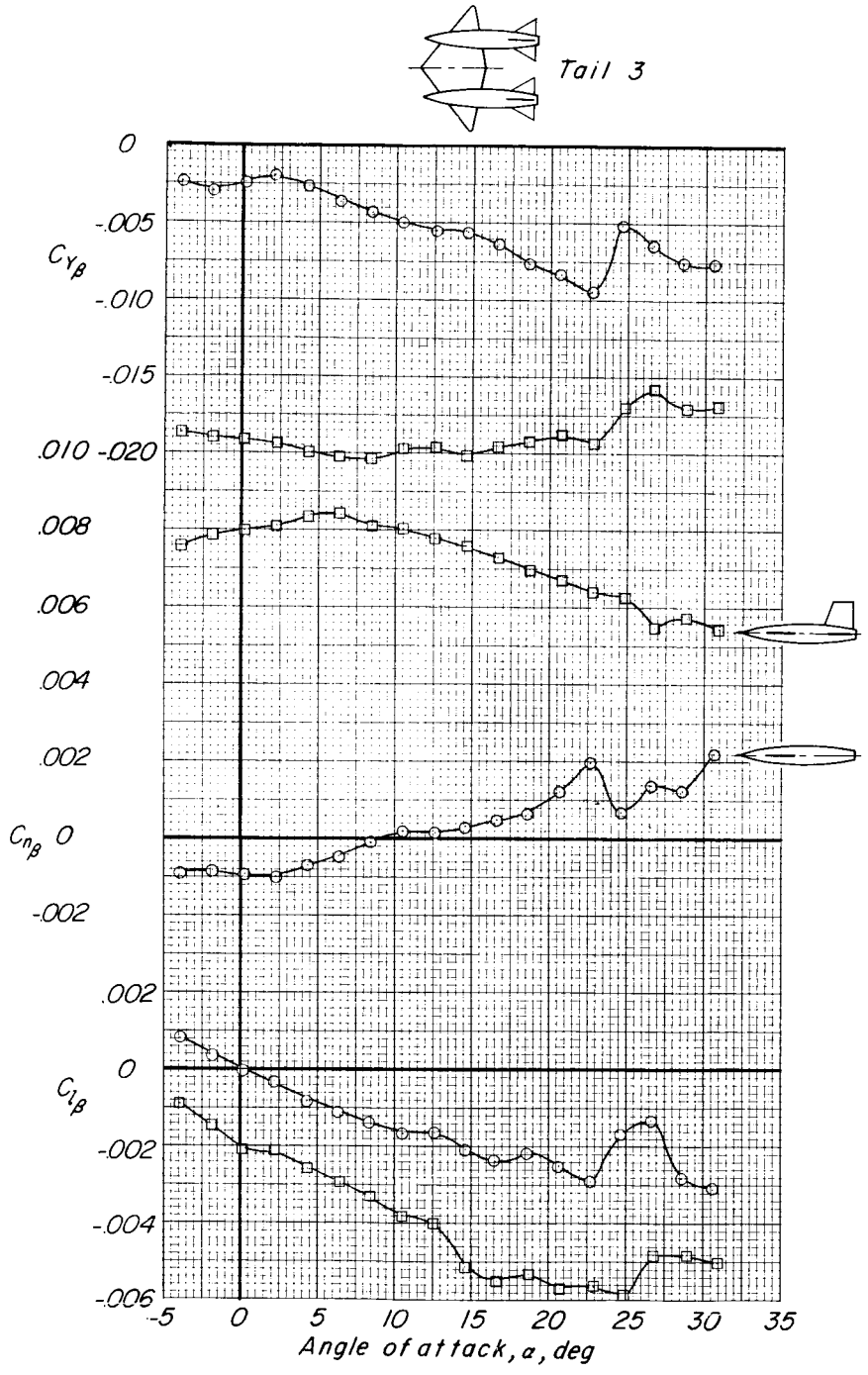

Figure 26.- Variation of static lateral stability derivatives with angle of attack for three-body model without center body with tail off and with tail 3.

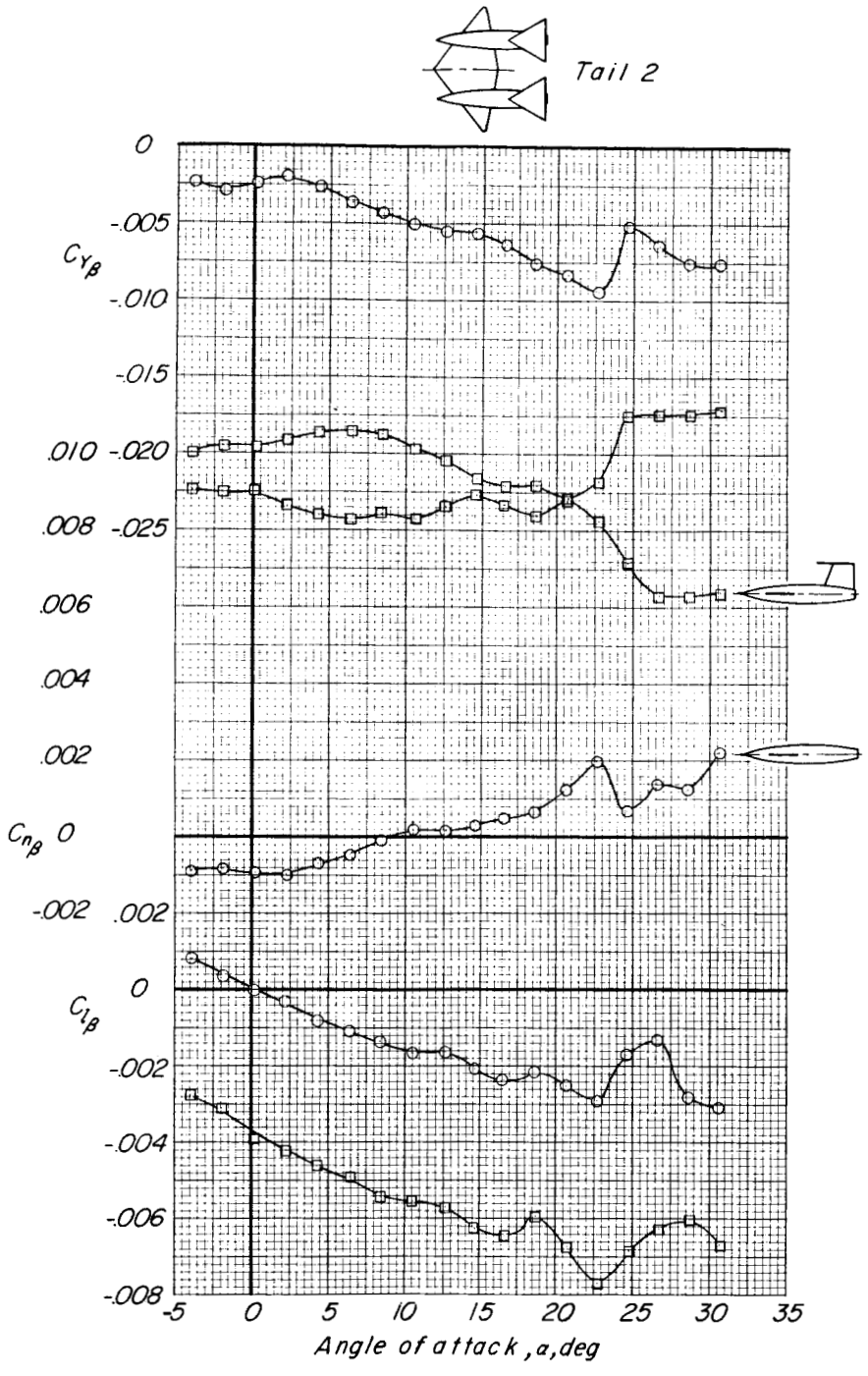

Figure 27.- Variation of static lateral stability derivatives with angle of attack for three-body model without center body and with tail off and with tail 2.

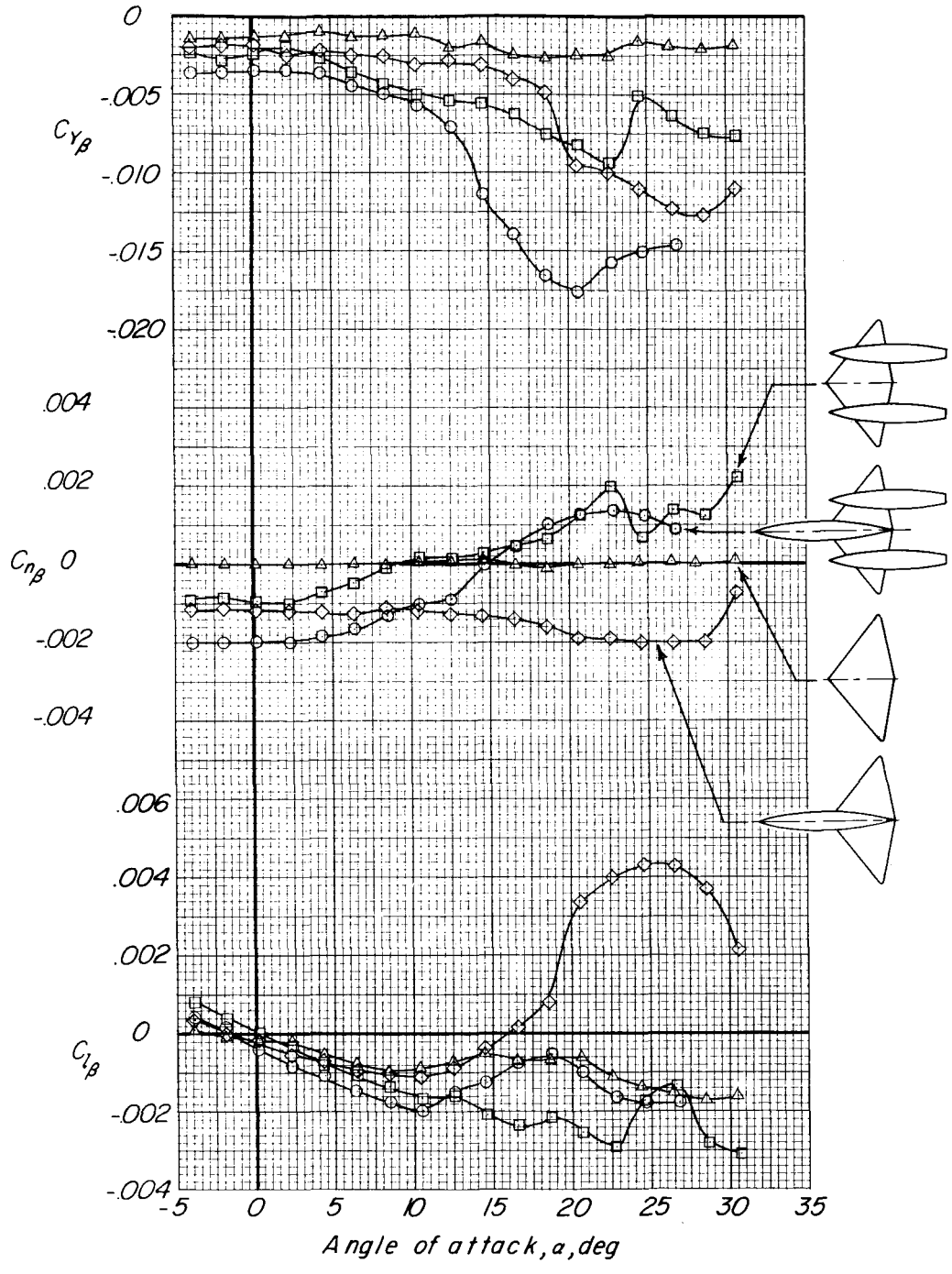

Figure 28.- Variation of static lateral stability derivatives with angle of attack for wing alone and wing in combination with one, two, or three bodies of three-body model.

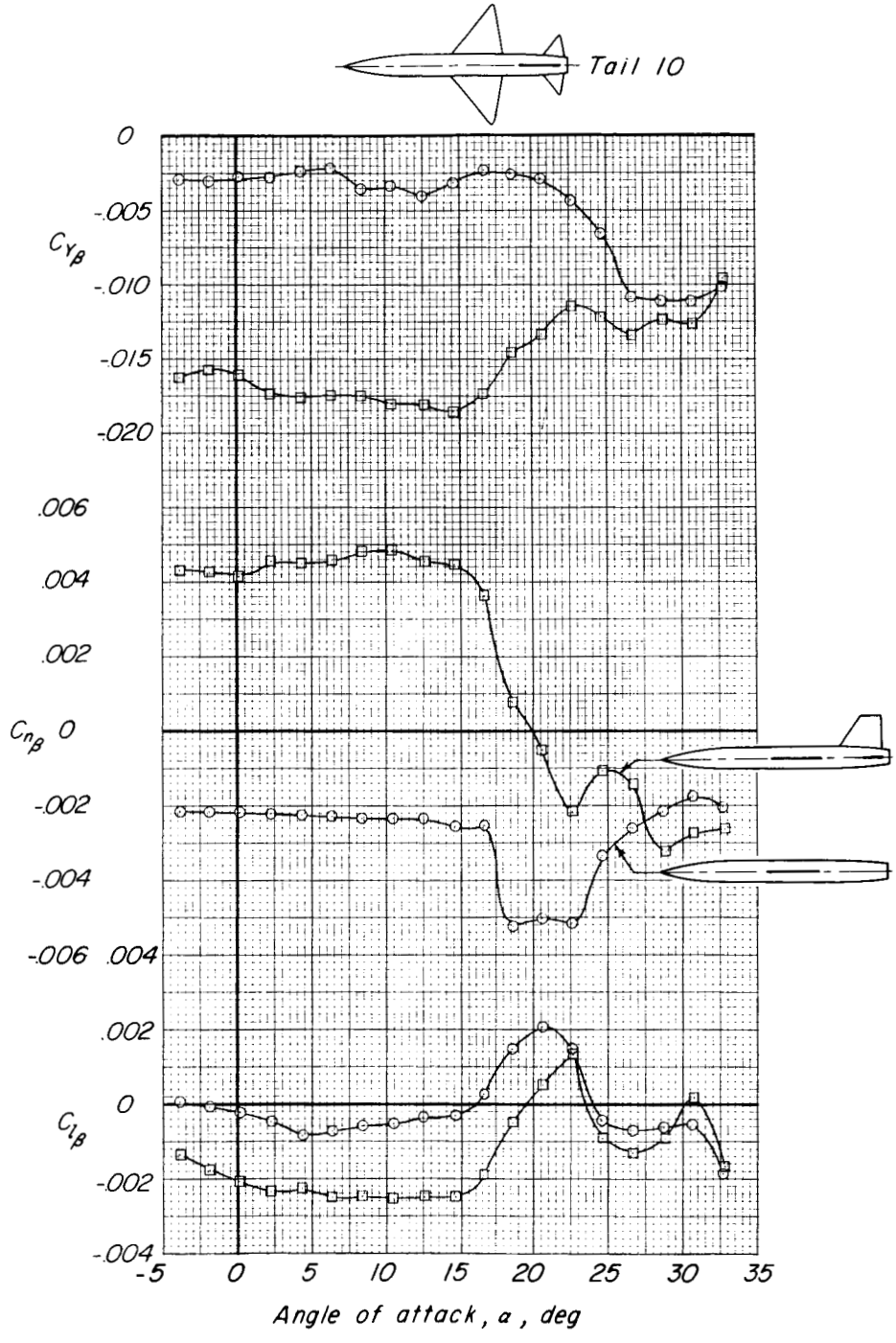

Figure 29.- Variation of static lateral stability derivatives with angle of attack for conventional wing-fuselage combination with tail off and with tail 10.

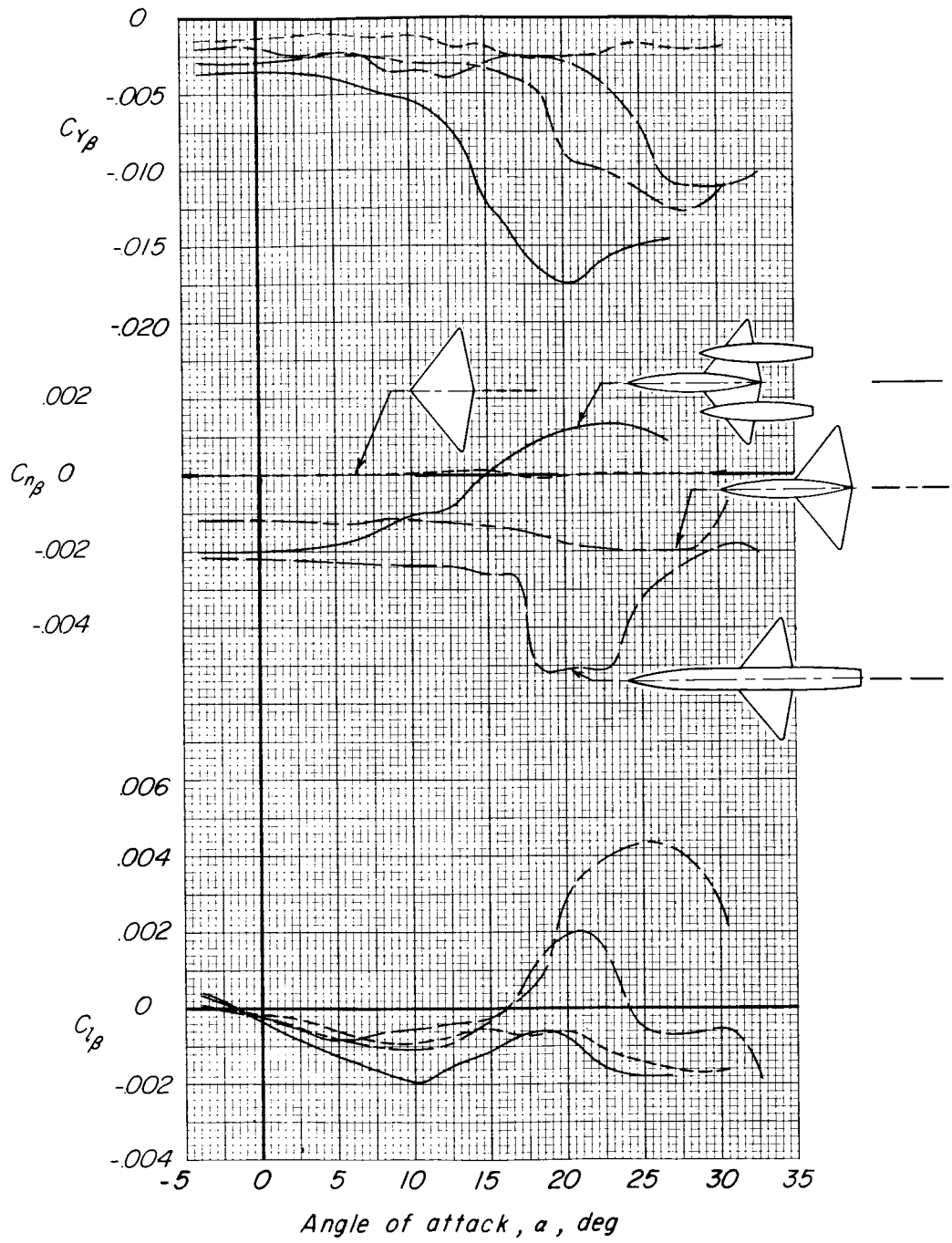

Figure 30.- Effect of body arrangement on static lateral stability derivatives compared with the conventional wing-fuselage model.

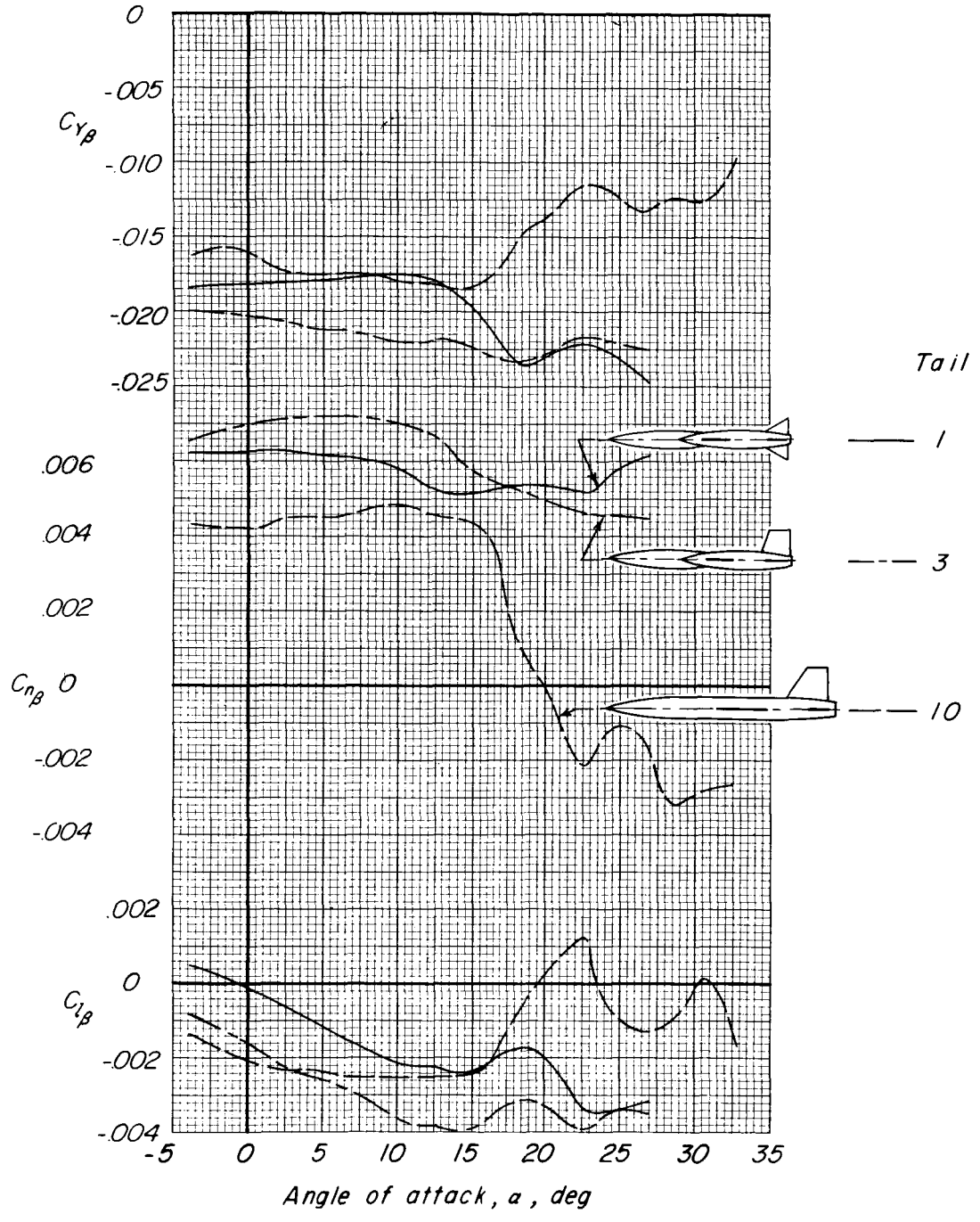

Figure 31.- Comparison of static lateral stability derivatives for two representative complete three-body model configurations with complete conventional model.

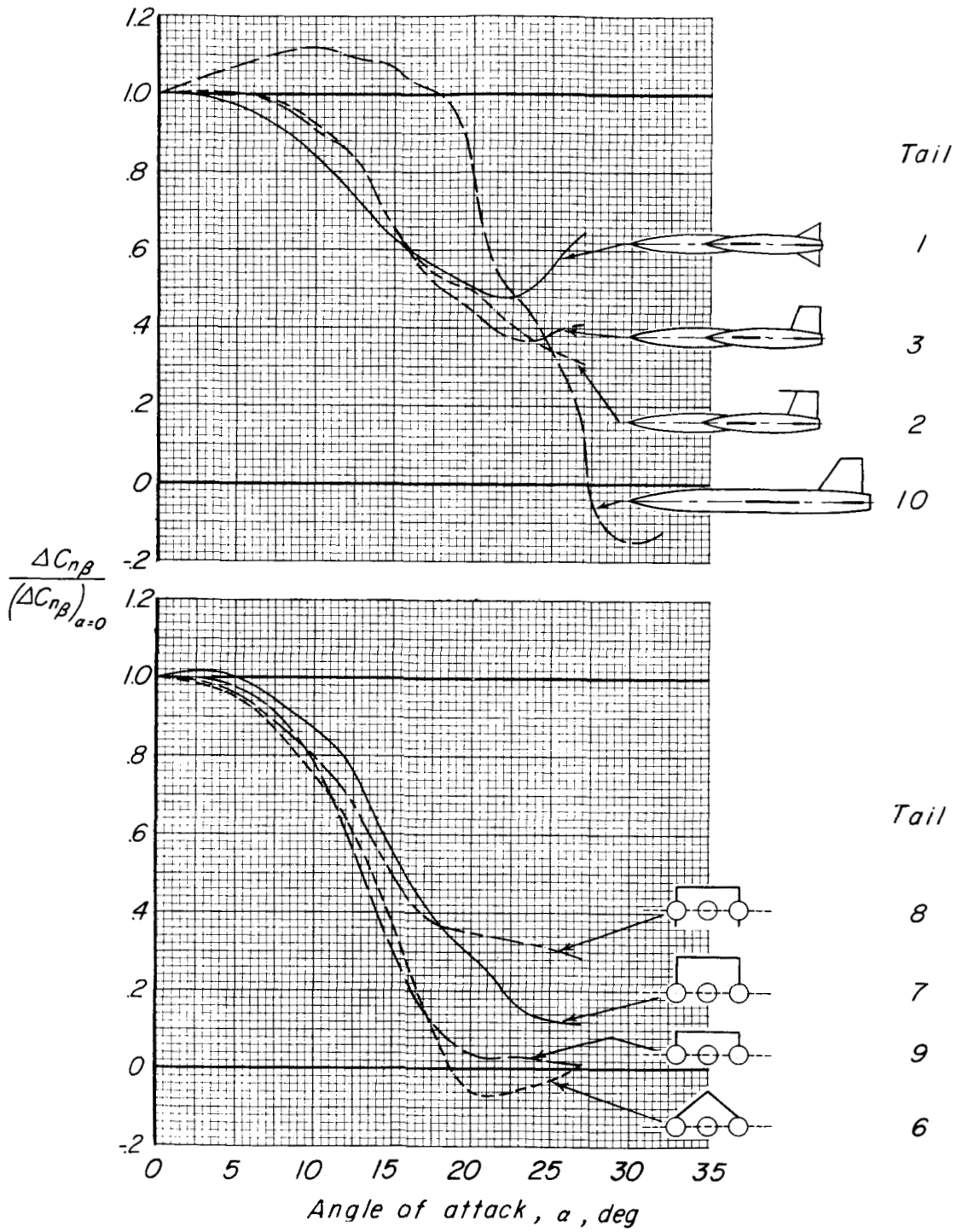

Figure 32.- Vertical-tail contribution to static directional stability derivative.